A re-examination of the mechanism of whiting events: A new role for diatoms in Fayetteville Green Lake (New York, USA)

Short running title: Re-examining whiting events in Fayetteville Green Lake

Authors and affiliations:

Chloe Stanton[1], Julie Cosmidis[1,2,*], and Lee R. Kump[1,2]

[1]Department of Geosciences, The Pennsylvania State University, University Park, PA 16802, USA
[2]Earth and Environmental Systems Institute, The Pennsylvania State University, University Park, PA 16802, USA
*Current address: Department of Earth Sciences, University of Oxford, Oxford OX1 03N, UK

Correspondence:
Julie Cosmidis, Department of Earth Sciences, University of Oxford, Oxford OX1 03N, UK.
Email: Julie.comidis@earth.oc.ac.uk.
Twitter : @JCosmidis

Key words:
Whitings, biomineralization, diatoms, calcite, micrite, ACC

ABSTRACT

Whiting events – the episodic precipitation of fine-grained suspended calcium cabonates in the water column – have been documented across a variety of marine and lacustrine environments. Whitings likely are a major source of carbonate muds, a constituent of limestones, and important archives for geochemical proxies of Earth history. While several biological and physical mechanisms have been proposed to explain the onset of these precipitation events, no consensus has been reached thus far. Fayetteville Green Lake (New York, USA), is a meromictic lake that experiences annual whitings. Materials suspended in the water column collected through the whiting season were characterized using scanning electron microscopy and scanning transmission X-ray microscopy. Whitings in Fayetteville Green Lake are initiated in the spring within the top few meters of the water column, by precipitation of fine amorphous calcium carbonate (ACC) phases nucleating on *Synechococcus* cells (cyanobacteria), as well as on extracellular polymeric substances (EPS), including abundant β-chitin fibrils exuded by centric diatoms. Whiting particles found in the summer consist of 5-7 μm calcite grains forming aggregates with diatoms and their EPS. Simple calculations demonstrate that calcite particles continuously grow over several days, then sink quickly through the water column. In the late summer, partial calcium carbonate dissolution is observed deeper in the water column. Settling whiting particles however reach the bottom of the lake, where they form a major constituent of the sediment, along with diatom frustules. The importance of diatoms and their EPS in whitings at Fayetteville Green Lake is described for the first time here, a largely overlooked mechanism for other whiting events in modern and ancient environments.

1. INTRODUCTION

Fine-grained (micritic) limestone is abundant in the sedimentary record and an important repository for geochemical and isotopic proxy records of Earth history. Despite its importance, the origin of marine mud has been a topic of considerable uncertainty and research for decades (Bathurst, 1966), with both inorganic and biogenic mechanisms being proposed. One source of mud, the apparently spontaneous precipitation of very fine suspended calcium carbonate ($CaCO_3$) particles, called a whiting, has been observed to occur and persist for many days in marine environments, most notably in the Bahamas (Broecker & Takahashi, 1966; Shinn *et al.*, 1989; Robbins *et al.*, 1997; Purkis *et al.*, 2017). Physical disturbance and re-suspension of carbonate sediments (e.g., Boss & Neumann, 1993; Broecker *et al.*, 2000; Morse *et al.*, 2003; Dierssen *et al.*, 2009; Broecker, 2012), chemical precipitation (Brunskill, 1969), and biological mediation (e.g., Robbins & Blackwelder, 1992; Thompson, 2000; Swart *et al.*, 2014; Long *et al.*, 2017) have been proposed to explain the whiting phenomenon.

1.1 Biological hypotheses for the origin of whitings

Among biological mechanisms, a role of photosynthetic microorganisms (in particular, cyanobacteria) has often been invoked for whiting production, supported by the fact that whiting events often coincide spatially and temporally with high abundances of these organisms (Schultze-Lam *et al.*, 1997; Hodell *et al.*, 1998; Thompson, 2000; Dittrich *et al.*, 2004; Dittrich & Obst, 2004). Biological models for the onset of whitings frequently involve the heterogeneous nucleation of $CaCO_3$ minerals on microbial surfaces and extracellular organic materials in supersaturated waters (Robbins & Blackwelder, 1992; Schultze-Lam *et al.*, 1992; Thompson, 2000). Picocyanobacteria in particular, because of their small sizes, offer a larger surface area for $CaCO_3$

nucleation (Robbins & Blackwelder, 1992; Hodell *et al.*, 1998; Dittrich *et al.*, 2004; Dittrich & Obst, 2004). Some studies have focused more specifically on the role of the S-layer of picocyanobacteria of the genus *Synechococcus*. Forming a hexagonally symmetric paracrystalline surface array, the S-layer may act as a template favoring calcite nucleation at the cell surface (Thompson & Ferris, 1990; Schultze-Lam *et al.*, 1992, 1997; Thompson, 2000).

In addition to models based on $CaCO_3$ nucleation on microbial surfaces ("passive" mineralization), cyanobacteria and other photosynthetic organisms might also provoke whiting events by locally increasing supersaturation with respect to calcium carbonates though CO_2 uptake ("active" mineralization) (Schultze-Lam *et al.*, 1997; Thompson, 2000; Dittrich & Obst, 2004). Recently, Lisle & Robbins (2016) hypothesized that viral lysis of cyanobacterial cells releases cytoplasmic bicarbonate – which is 23 times more concentrated in the cytoplasm than in seawater – leading to extreme mineral supersaturation in the immediate vicinity of the cells, and enabling homogeneous nucleation of $CaCO_3$.

Other mechanisms for microbial precipitation of $CaCO_3$ minerals have been described in the literature dealing with calcifying microbial mats and microbialites (*e.g.*, Dupraz & Visscher, 2005; Dupraz *et al.*, 2009; Zhu & Dittrich, 2016). Some of these mechanisms, such as bacterial sulfate reduction or anoxygenic photosynthesis, are irrelevant to whiting events, which occur in the oxygenated photic zone of the water column. Others, such as the degradation of microbial EPS locally releasing calcium and carbonate ions, could be relevant to planktonic $CaCO_3$ formation, but it is not clear whether such mechanisms could be playing a role in the onset of whitings. Finally, some cyanobacteria (Benzerara *et al.*, 2014) as well as other bacterial types (Benzerara *et al.*, 2021; Monteil *et al.*, 2021) and microalgae (Martignier *et al.*, 2017) can form amorphous intracellular

calcium carbonate biominerals, but their involvement in whiting events has never been documented.

1.2 A role of diatoms in whitings?

Several studies have described an association of planktonic and benthic $CaCO_3$ precipitation with diatom species in different marine and lacustrine environments (Winsborough & Golubić, 1987; Küchler-Krischun & Kleiner, 1990; Winsborough, 2000; Ehrlich *et al.*, 2016; Fuchs *et al.*, 2016; Long *et al.*, 2017; Gomez *et al.*, 2018). Diatoms can produce large amounts of extracellular polymeric substances (EPS), also called mucilage, playing different roles such as adhesion, motility, protection, and heavy metals detoxification (Urbani *et al.*, 2012; Shnyukova & Zolotareva, 2015). In oligotrophic hardwater lakes, diatoms have been observed in increasing numbers, causing ecological strain (Kirkwood *et al.*, 2007; Novis *et al.*, 2017), and their abundance sometimes coincides with increased sedimentation of $CaCO_3$ (Stabel, 1986; Fuchs *et al.*, 2016). In at least one marine environment (southwest Florida), $CaCO_3$ whiting particles where associated with centric diatoms (Long *et al.*, 2017), but it is unclear whether diatoms or their EPS could be a significant factor in calcium carbonate nucleation in other modern whiting events.

1.3 Whiting events at Fayetteville Green Lake

Fayetteville Green Lake (FGL) (NY, United States) is a 53 m deep, permanently stratified lake where annual whitings have been documented. The lake redoxcline at ~20 m water depth separates an upper, wind-mixed, oxygenated mixolimnion from a lower, slightly denser, euxinic monimolimnion (Takahashi *et al.*, 1968). The surface waters of FGL are supersaturated with respect to calcite ($\Omega \approx 10$) (Takahashi *et al.*, 1968), and experience a whiting every spring, when

109 precipitation of fine-grained suspended calcite transforms the lake color from deep blue to
110 turquoise (Thompson *et al.*, 1990; Schultze-Lam *et al.*, 1997).

111 Previous investigations of FGL documented the evolution of the whiting over time
112 (Schultze-Lam *et al.*, 1997), and showed that the initiation of the whiting in the spring (May)
113 roughly coincides with an annual cyanobacterial bloom. Carbon stable isotope measurements in
114 the water column and the sediment of the lake further suggest that photosynthesis-driven carbonate
115 precipitation in the mixolimnion is the primary source of carbonate minerals in the sediments
116 (Schultze-Lam *et al.*, 1997; Havig *et al.*, 2017). A model for the onset on the whiting has been
117 proposed in the 1990s, in which *Synechococcus* (micron-sized coccoid cyanobacteria) were the
118 main biological agents driving $CaCO_3$ precipitation. The cyanobacteria are thought to be driving
119 local increases of saturation state from their photosynthetic activity, and acting as sites for mineral
120 nucleation (Thompson *et al.*, 1990; Schultze-Lam *et al.*, 1997). A *Synechococcus* strain isolated
121 from FGL was shown in the laboratory to nucleate calcite crystals at the cell surface, possibly
122 templated on the S-layer (Thompson & Ferris, 1990; Schultze-Lam *et al.*, 1992). Recently,
123 Kamennaya *et al.* (2020) have shown that *Synechococcus* thriving in the surface waters of FGL
124 produce abundant EPS that can adsorb diverse cations (including calcium) and detach from the
125 cells. However, it is not clear whether or not these cell-free calcium-loaded EPS envelopes play a
126 role in triggering whitings at FGL.

127 Other recent studies on FGL have focused on thrombolitic microbialites growing on the
128 lake shore (DeMott *et al.*, 2020), isotopic fractionation effects associated with microbial calcite
129 precipitation (Chen *et al.*, 2021), as well as carbon and nitrogen biogeochemical cycling (Havig *et*
130 *al.*, 2017; Fulton *et al.*, 2018), sulfur biogeochemistry (Zerkle *et al.*, 2010; Oduro *et al.*, 2013), and

microbial and geochemical processes at the chemocline and in the monimolimnion (Meyer *et al.*, 2011; Hunter, 2012; Havig *et al.*, 2015; Rojas *et al.*, 2021).

We performed a high-resolution microscopy and spectroscopy characterization of particles suspended in the water column of FGL and collected through the whiting season, as well as of particles from the lake bottom sediments, enabling us to propose new hypotheses for the biological mechanisms involved in whiting events and carbonate sedimentation.

2. METHODS

2.1 Field sampling

Field work was conducted during the spring, summer, and fall of 2018 at Green Lakes State Park, in Fayetteville, NY (United States). Five field trips were executed on April 16, May 31, June 30, August 1, and September 8 of 2018. Samples were collected from a boat stationed near the lake center. Water samples were collected using a peristaltic pump at every 1 m interval for the top ~10 m of the water column. Both filtered (0.2 µm polycarbonate filters) and unfiltered water samples were collected and stored at 4°C. Polycarbonate filters were immediately rinsed with deionized (DI) water, air-dried, and stored for later microscopy analyses. Sediment trap samples analyzed in this study were collected by S. Romaniello (University of Tennessee, Knoxville) between July 12 and July 21, 2017 from 13.5 depth, and stored at -20°C prior to analyses. Samples from the top 4 inches of a Green Lake bottom sediment core were also analyzed. These sediment core samples were freeze-dried for preservation. They have been further described elsewhere (Havig *et al.*, 2015, 2017).

2.2 Scanning Electron Microscopy (SEM)

Suspended particles from the water column and collected on polycarbonate filters, as well as rinsed sediment trap samples, were characterized using scanning electron microscopy (SEM) on a FEI Nova NanoSEM 630 field emission gun SEM. Elemental information was derived from Energy-dispersive X-ray Spectroscopy (EDS) (Oxford Instruments UltimMax detector) to confirm the mineralogy of observed particles. Images were collected at accelerating voltages ranging from 5-15 keV and at working distances down to 3 mm, while EDS analyses were conducted at 15 keV at working distances down to 7 mm. EDS data was processed using the program Oxford Aztec.

Mineral morphology and texture, size, and abundances, as well as diatom abundances were assessed using SEM images generated throughout the whiting season by manual counting on ~700 μm x 700 μm SEM images of the filters. Three types of particles were counted and measured on these large-scale overview images: pennate diatoms, centric diatoms, and carbonate grains. The visual aspect of the carbonate particles was furthermore characterized as either intact or pitted (as indicative of dissolution). Once all particles on these larger images had been counted, the volumetric concentrations of each type of particle was calculated, using the volume of filtered water for each filter and filter area. The areas counted (~0.49 mm^2) were assumed to be representative of the entire filters (~490 mm^2), which contained all particles from the originally filtered 60 mL samples. Using these values, particle counts from the SEM images were converted into concentrations of particles per milliliter.

2.3 Scanning Transmission X-ray Microscopy (STXM)

2.3.1 STXM data acquisition and processing

Scanning Transmission X-ray Microscopy (STXM) was used to collect spectroscopic data on the sub-micrometer scale distribution and speciation of carbon and calcium in minerals and associated organics. STXM analyses were performed on beamline SM at the Canadian Light Source, Saskatoon, SK, operating with a 35 nm zone plate (ZP) on samples collected from the water column in April 2018. Another beamtime at the STXM beamline 5.3.2.2 (operating with a 25 nm ZP) of the Advance Light Source, Berkeley National Lab, CA, was used to analyze sediment trap and sediment core samples. For STXM, particulate materials were centrifuged, rinsed with deionized water, and deposited onto silicon nitride windows (Norcada).

STXM data acquired at the C K-edge and Ca $L_{2,3}$-edge were processed in aXis2000 (Hitchcock, 2012). Transmission images were first converted to optical density (OD). At the C K-edge, organic carbon maps were generated by subtracting an OD image at 280 eV (below the C K-edge) from another at 288.2 eV (absorption energy of 1 $s \rightarrow \pi^*_{C=O}$ electronic transitions in amide groups). Calcium maps were obtained at the Ca $L_{2,3}$-edge by subtracting an OD image at 343 eV (below the Ca L_3-edge) from another at 349.3 eV (energy of the Ca L_3-edge).

X-ray absorption near edge structure (XANES) spectra were extracted from image stacks according to the procedure described by Cosmidis & Benzerara (2014). The Stack Fit tool of aXis2000 was used to extract and map the distribution of representative components in image stacks. Linear background removal was performed on XANES spectra in the 270-283 eV energy range below the C K-edge and the 340-346 eV energy range below the Ca $L_{2,3}$-edge.

2.3.2 Determination of I_C/I_{Ca} ratios

XANES spectra at the C K-edge and Ca $L_{2,3}$-edge were used to obtain a semi-quantitative measure of elemental ratios of carbon versus calcium in the samples. The I_C/Ic_a ratio is defined as the ratio of the areas under the spectra in the 280-310 eV region versus the 345-354 eV region

(Fig. 1a). I_C/Ic_a ratios measured on different calcium-bearing reference samples with known elemental compositions showed good correlation with C/Ca molar ratios (Fig. S2) ($R^2 \sim 0.95$) (Fig. 1b). The reference compounds included carbonate minerals (amorphous calcium carbonate, aragonite, benstonite, calcite, dolomite), calcium-phosphate minerals (francolite, hydroxyapatite), and *Escherichia coli* cells, and have already been described elsewhere (Benzerara *et al.*, 2004; Cosmidis & Benzerara, 2014; Cam *et al.*, 2015; Cosmidis *et al.*, 2015a, 2015b).

I_C/Ic_a ratios were used to distinguish calcium carbonate mineral phases (empirically defined as I_C/Ic_a <3.3) from organic materials with adsorbed Ca^{2+}. The presence of X-ray absorption features at 290.3 eV and around 301.5 eV was furthermore used to discriminate calcium-carbonate minerals from organic matter (absorbing in the 285.0-288.7 eV range) (Brandes *et al.*, 2010) (Fig. 1a). A more quantitative assessment of carbonates versus organic carbon concentrations was not attempted due to the fact that the intensity of the X-ray absorption signal 290.3 eV ($1s \rightarrow \pi^*$ electronic transitions in carbonate groups) in carbonate minerals depends on the orientation of the crystals with respect to the X-ray beam (Metzler *et al.*, 2008).

2.3.3 Determination of calcium carbonate crystallinity: splitting ratios at the Ca $L_{2,3}$-edge

Calcium carbonate mineral phases were identified by comparison with reference spectra at the Ca $L_{2,3}$-edge. The crystallinity of calcium carbonates was furthermore quantified using calculated splitting ratios (SRL_2, SRL_3), which provide a measure of the crystal field splitting at the Ca L_2 and L_3 edges, as defined in Politi *et al.* (2008). Typically, the Ca $L_{2,3}$-edge spectra of amorphous calcium carbonates (ACC) have poorly split L_2 and L_3 peaks, while the spectra of crystalline phases such as calcite display higher SRL_2 and SRL_3 splitting ratios characteristic of well resolved split peaks (Politi *et al.*, 2008) (Fig. 1c).

3. RESULTS

3.1 Types and abundances of whiting particles

SEM was used to image and quantify the abundance of solid particles collected on filters at different depths in the FGL water column throughout the 2018 whiting season. Sampled particles primarily consist of centric and pennate diatoms, carbonate minerals grains, microbial cells, and extracellular organic materials (Figs. 2, S1). Calcium carbonate minerals are not visible in SEM images in April but are present in June, with highest abundances in the 3 m sample, showing the shallow location of the whiting in the water column (Fig. 3). Both centric and pennate diatoms increase in numbers as the summer progresses, peaking in June, while the abundance of carbonate minerals peaks in August. Unfortunately, abundances of microbial cells (e.g. cyanobacteria) cannot be quantified using SEM images, due to their small sizes and low density to the electron beam. Both calcium carbonate minerals and diatoms sink deeper in the water column with time, evidenced by counts showing decreasing abundance in the shallow water column and increasing abundance at greater depth through the summer. The aspect of carbonate minerals changes through time, as depicted in Figure 2a-c: early carbonate grains (June) appear smooth, while later carbonate grains (August) develop pitted, rough outer surfaces as well as rounder shapes. Howver, the average size of suspended carbonate grains remains relatively constant with time (~5-7 μm in length) through the whiting. Carbonate grains and diatoms are found within a mesh of long organic filaments, ~100 nm thick, likely corresponding to β-chitin fibrils produced by some centric diatoms (Herth & Barthlott, 1979; Gügi *et al.*, 2015; Novis *et al.*, 2017). These fibrils are also observed aggregated with carbonates and diatoms in sediment trap samples collected at 13 m depth in July 2017 (Fig. 2f, S2). Some centric diatoms from the water column samples appear to be extruding EPS materials through pores of their silica valves (Fig. 1d). The brightness of this exuded material

in SEM images suggests that it might be associated with heavy elements such as absorbed metallic cations.

3.2 Calcium carbonate mineralogy and calcium association with cells and organics

3.2.1 Pre-whiting samples from the FGL water column (April)

Samples collected from the FGL water column at 8 m depth in April 2018 (before the onset of conspicuous calcium carbonate precipitation) were analyzed using STXM at the C K- and Ca $L_{2,3}$-edges. Abundant centric diatoms were observed, confirming SEM results, along with spherical and rod-shaped microbial cells (Fig. 4). The spherical cells are relatively small (~0.8 µm in diameter), and likely correspond to cyanobacteria of the genus *Synechococcus,* the dominant autotrophs in Green Lake (Thompson *et al.*, 1990; Schultze-Lam *et al.*, 1997; Kamennaya *et al.*, 2020). Diatoms and bacteria are found amidst extracellular organic material, forming either fibrils or thin films, and interpreted as EPS produced by microbial cells and/or diatoms. Note that this EPS material, although visible on STXM transmission images, do not always appear on organic carbon maps, likely due to their extreme thinness (possibly 10 nm or thinner; Svetličić *et al.*, 2013) which might prevent the obtention of a proper focus of the X-ray beam and good absorption signal.

C K-edge XANES spectra obtained on *Synechococcus* cells exhibit a main peak at 288.2 eV (amide groups in peptides), with smaller peaks at 285.0-285.5 eV (aromatics and unsaturated carbon), and shoulders at 286.6 eV (ketonic and phenolic groups), 287.4 eV (aliphatics, phenols and/or ketones), 288.5 eV (carboxylic groups), 289.4 eV (hydroxyl groups, ethers, and/or C=O groups in nucleic acids), and 290.3 eV (carbonate groups) matching previously published bacterial spectra (e.g, Benzerara *et al.*, 2004; Chan *et al.*, 2011; Cosmidis *et al.*, 2015a) (Fig. 5).

In contrast, the C K-edge spectra of the EPS show a main peak at 288.5 eV (carboxylic groups), consistent with a composition dominated by acidic polysaccharides (Lawrence *et al.*, 2003; Chan *et al.*, 2009; Mitsunobu *et al.*, 2014), with smaller peaks and shoulders around 285.0-285.5 eV (aromatics and unsaturated carbon), 287.4 eV (aliphatics, phenols and/or ketones), 288.2 eV (amide groups), and 289.4 eV (hydroxyl groups, ethers, and/or C=O groups in nucleic acids). Note that peaks at 288.5 and 289.4 eV are also consistent with the presence of β-chitin (Lehmann *et al.*, 2009), which composes the EPS fibrils extruded by many centric diatoms (Herth & Barthlott, 1979; Novis *et al.*, 2017).

At the Ca $L_{2,3}$-edge, STXM shows the presence of abundant calcium on EPS films and diatoms, in particular on perforations of the frustules, from which EPS are typically exuded (Herth & Barthlott, 1979) (Fig. 6). Relatively minor amounts of calcium are detected on microbial cells (see calcium maps on Fig. 4), where this element is only present as adsorbed Ca^{2+}, identifiable by a weak absorption signal at the Ca $L_{2,3}$-edge ($I_{C/Ca}$ ratios 10-50) and absence of strong peaks at 290.3 eV and 301.5 eV (corresponding to carbonates) at the C K-edge. The surfaces of the *Synechococcus* cells are enriched in adsorbed calcium compared with their interiors, which can be determined by comparing the intensity of the absorption signal at the C K-edge and Ca $L_{2,3}$-edge on the XANES spectra extracted from a cell interior (labelled S1) and cell surface (labelled L) on Figure 7. For instance, for the *Synechococcus* cell in Fig. 7a, I_C/I_{Ca} = 46 on the cell interior and I_C/I_{Ca} = 17 on the cell surface. The calcium enrichment of the cell surface may be indicative of Ca^{2+} adsorption on *Synechococcus* S-layers, as described in previous studies (Thompson & Ferris, 1990; Schultze-Lam *et al.*, 1992).

283 Calcium is furthermore enriched on EPS films, forming irregularly shaped dense clots
284 (white arrows on Fig. 4), displaying low I_C/I_{Ca} ratios ranging from 0.5 to 2.5, as well as intense
285 X-ray absorptions at 290.3 eV and ~301.5 eV, and thus interpreted as calcium carbonate
286 minerals. At the Ca $L_{2,3}$-edge, their calculated splitting ratios are SRL_3 ~1.2-1.4 and SRL_2 ~ 1.3-
287 1.4, matching a reference amorphous calcium carbonate (ACC) (Fig. 8). ACC in the pre-whiting
288 samples is also found as small (<500 nm) mineral grains located on or nearby *Synechococcus*
289 cells (phases mapped in blue in Fig. 7). These ACC phases were not identified on SEM images,
290 possibly due to their small sizes.
291 Calcium is also concentrated in round-shaped areas within the EPS films, measuring ~1
292 µm in diameter (open arrows in Fig. 4d,f; Fig. S3a). Due to their weak signal at the Ca $L_{2,3}$-edge
293 as compared with ACC grains described above, they likely correspond to adsorbed Ca^{2+} on
294 organic material rather than to calcium-carbonate minerals. No XANES spectra were acquired on
295 these objects, preventing calculations of I_C/I_{Ca} ratios. These round shaped calcium enrichments
296 may correspond to "bag-like" EPS envelopes issued from *Synechococcus* cells, which can
297 dissociate from the cells and have high Ca^{2+} adsorption capacity (Kamennaya *et al.*, 2020).
298 ***3.2.2 Whiting sample (sediment trap)***
299 STXM analyses were performed on whiting particles collected in a sediment trap placed
300 in the FGL water column at 13.5 m depth between July 12 and July 21, 2017. The sample
301 contains abundant calcium carbonate particles, measuring up to 7 µm in length, and identified as
302 calcite based on the similarity of their Ca $L_{2,3}$-edge XANES spectra with that of a reference
303 calcite (Fig. 9, S4), in agreement with previous studies of whitings at FGL (Thompson *et al.*,
304 1990; Schultze-Lam *et al.*, 1997). Calculated I_C/I_{Ca} ratios for these calcite grains range between
305 2.5 and 3.3, and splitting ratios at the Ca $L_{2,3}$-edge are SRL_2 ~ 1.6-1.7 and SRL_3 ~1.8-2.0 (Fig.

306 8), consistent with crystalline calcite (Politi *et al.*, 2008). C K-edge XANES spectra obtained on
307 the calcite grains sometimes display absorption peaks at 288.2-288.5 eV (amides and
308 carboxylics), suggesting that organic compounds may be adsorbed onto or incorporated within
309 the mineral particles (Fig. 9d).

310 The calcite grains are forming aggregates also containing centric diatoms and organic
311 material, present either as fibrils, or as organic particles surrounding the minerals.
312 *Synechococcus* cells were not observed in the sediment trap sample. The C K-edge XANES
313 spectra of the organic fibrils and particles display main peaks at 288.5 eV (carboxylic groups)
314 and 288.2 eV (amide groups), with smaller peaks or shoulders at 285.0 and 285.5 eV (aromatics
315 and unsaturated carbon), 286.6 eV (ketonic and phenolic groups), 287.4 eV (aliphatics, phenols
316 and/or ketones), 289.4 eV (hydroxyl groups, ethers, and/or C=O groups in nucleic acids). This
317 composition is similar to that of EPS and diatom β-chitin fibrils previously described in pre-
318 whiting samples from the water column, with an increased contribution from amide groups
319 which may be derived from proteins issued from decomposing microbial cells. The organic
320 fibrils and particles display high I_C/I_{ca} ratios (73-605) and no absorption signal from carbonates
321 at the C K-edge, showing that calcium is only present as minor amounts of adsorbed Ca^{2+}.
322 Similarly, the diatoms display C K-edge XANES spectra consistent with cellular material with
323 main absorption features characteristic of amides and carboxylic groups and absence of strong
324 carbonate signal, with relatively high I_C/I_{ca} ratios (e.g. I_C/I_{ca} = 61 for the diatom fragment in Fig.
325 S4) consistent with the presence of adsorbed Ca^{2+} only.

326 ***3.2.3 Sediment core samples***

327 STXM analyses of sediment core samples from the bottom of FGL are presented in
328 Figure 10 as well as Supplementary figures S5 and S6. The sediment contains abundant calcium

carbonate grains, identified as calcite based on their Ca $L_{2,3}$-edge spectroscopic signature, and similar in shape and size with those observed in the whiting samples. This observation is consistent with isotopic studies suggesting that carbonate precipitation in the oxic zone of the lake is the primary source of carbonate in the sediments (Havig *et al.*, 2017). I_C/I_{Ca} ratios measured on the sediment calcite particles range between 2.1 and 2.6, and splitting ratios at Ca $L_{2,3}$-edges are SRL_3 ~ 1.9-3.2 and SRL_2 ~ 1.8 and 2.2 (SRL_2) (Fig. 8), indicating increased crystallinity compared with the whiting calcite particles from the sediment trap. C K-edge XANES spectra obtained on these sedimentary calcite particles display peaks at 288.2-288.5 eV, again showing possible adsorption of incorporation of organic molecules.

Abundant diatoms, sometimes fragmented, are also observed in the sediment. Diatoms are mostly centric, with fewer pennate forms (e.g., Fig 10c, S5). The diatoms are associated with higher amounts of calcium compared with diatoms from the sediment trap, as visible on STXM calcium maps. This abundance of calcium is reflected in low I_C/I_{Ca} ratios ranging from 3.4 to 7.5. Combined with strong absorption signals at 290.3 eV at the C K-edge (see in particular Fig. S6b), low I_C/I_{Ca} ratios indicate the presence of fine calcium carbonate phases associated with the diatoms frustules. Calculated splitting ratios at the Ca $L_{2,3}$-edge range between those of ACC and calcite (SRL_2 ~1.3-1.6 and SRL_3 ~1.1-1.5), corresponding to either ACC or poorly crystalline calcite.

Organic matter in the sediment samples is found in diatoms and rare extracellular fibrils (Fig. S5), as well as dense organic-rich particles found around diatoms and calcite grains, measuring up to ~5 µm (see one of these large organic particles in Fig. S6). These organic particles have a C K-edge signature similar to that of organic particles in the sediment traps.

4. DISCUSSION

4.1 Biological mechanisms in the FGL whiting

The whiting at FGL corresponds to the conspicuous precipitation of calcite crystals in the shallow water column of the lake, first observed at ~3 m depth in June (although find ACC grains are present associated with organics are present as early as April). Calcite saturation indices of ~1 at the surface of FGL (Takahashi *et al.*, 1968; Havig *et al.*, 2015) can be compared to indices of ~0.3 in waters of the Bahama Banks (Broecker & Takahashi, 1966), where marine whitings are regularly observed. Previous work has suggested that variability in saturation state leads to measurable changes in whiting precipitation rates (Morse *et al.*, 2003), suggesting that precipitation rates at FGL have the potential to be fast in comparison to marine whitings. It is unclear whether or not photosynthetic organisms such as cyanobacteria and diatoms play a role in calcite precipitation through CO_2 uptake and localized alkalinization. Indeed, calcite abundances (peaking at ~4 m depth in August) are uncorrelated with maximum abundances of diatoms (at ~8 m in June) (Fig. 3), and previous studies found no correlation in space and time between peak abundances of calcite and *Synechoccus* (Schultze-Lam *et al.*, 1997).

However, it is obvious that organic-mineral interactions involving microbial cells and EPS play a crucial role in calcium carbonate mineralization at the onset of the whiting. In April, STXM analyses reveal fine ACC phases covering abundant EPS derived from diatoms (Fig. 6), as well as cyanobacterial cells (*Synechococcus*) (Fig. 7). The precipitation of ACC minerals is likely facilitated by the adsorption of Ca^{2+} on organic surfaces such as *Synechococus* cells (Fig. 7), diatom EPS exuded from apertures of the silica valves (Figs. 2d, 6), and possibly "bag-like" empty EPS envelopes detached from *Synechococcus* cells (Fig. 4d,f) (Kamennaya *et al.*, 2020). A significant portion of the diatom EPS likely consists of β-chitin fibrils, found associated with

374 calcite particles later in the summer (Figs. 2, S2). This interpretation is supported by the fact that
375 microorganisms degrading chitin have been described in the FGL monimolimion (Rojas *et al.*,
376 2021).

377 At the molecular level, adsorption of Ca^{2+} ions can occur on negatively charged
378 functional groups such as deprotonated carboxylic groups in acidic polysaccharides and proteins.
379 In FGL waters, at pH 6-8, carboxyl groups exist in a deprotonated state (Beveridge, 1981), and
380 photosynthetic CO_2 uptake may result in local pH increases surrounding cyanobacteria and
381 diatoms, further facilitating deprotonation and calcium binding. Likewise, β-chitin molecules
382 forming an important part of diatom EPS present C=O, O–H, and N–H groups as well as oxygen
383 atoms with affinity for calcium ions, and chitin has been previously described as a nucleating
384 agent for both amorphous and crystalline calcium carbonate biominerals (Ehrlich, 2010).

385 While a role of *Synechococcus* S-layers in calcium carbonate nucleation and templating
386 has been proposed in earlier studies (Thompson & Ferris, 1990; Schultze-Lam *et al.*, 1992),
387 implication of diatom EPS in whiting at FGL is proposed here for the first time. Recent studies
388 have described spatial associations of centric diatoms with calcium-carbonates precipitates in the
389 water column of Lake Stechlin (Geramany) (Fuchs *et al.*, 2016) as well as in a southwest Florida
390 whiting event (Long *et al.*, 2017). In the second example, amorphous and crystalline $CaCO_3$
391 particles were observed along the diatom girdle bands, which was explained by the unique surface
392 chemistry and chemical microenvironment in this region of the diatom frustule associated with
393 cell division.

394 It is not clear why the role of diatoms and exuded EPS has been overlooked in previous
395 studies of the whitings at FGL. The high abundance of diatoms in the lake sediments (Figs. 10, S5,
396 S6) indicate that they have been thriving in past decades, and their presence is mentioned in several

older articles (Culver & Brunskill, 1969; Thompson *et al.*, 1990; Schultze-Lam *et al.*, 1997). Nano-particulate ACC nucleating on diatom EPS in the early spring may have been unnoticed in the past due to unsuitable observation techniques. It is also possible that whiting nucleation mechanisms at FGL have evolved over time, with varying contributions of cyanobacteria versus diatoms through the lake's recent history. Predominant mechanisms of calcium carbonate nucleation may shift depending on the microbial community dynamics in the water column, as a result of changes in climatic conditions and/or in the nutrient status of the lake.

In the summer, during the peak of the whiting, calcium carbonate is found as larger (up to ~7 µm) crystalline calcite grains, aggregating with diatoms as well as EPS materials including abundant β-chitin fibrils (Figs. 2, 9). It is unclear whether the whiting calcite particles correspond to the crystallization and growth of ACC particles observed in pre-whiting samples, although ACC is a common precursor phase to crystalline calcite in biological precipitation systems (Weiner *et al.*, 2005). In particular, ACC is a precuror phase for $CaCO_3$ mineralization on microbial EPS (Enyedi *et al.*, 2020; Shiraishi *et al.*, 2020). Intermediate phases between nano-ACC particles and calcite crystals measuring several micrometers in lengths were not observed, which may be due to fast calcite growth in supersaturated solutions (see next section of the discussion).

In the sediment trap sample (July), organic materials and diatoms associated with the calcite particles display very small amounts of adsorbed Ca^{2+} as compared with pre-whiting samples (see high I_C/I_{Ca} values in Figure 8). Low amounts of calcium adsorbed on organics and diatoms in this whiting sample may thus suggest that calcite minerals grown at the expense of Ca^{2+} initially adsorbed on biological materials.

418 **4.2 The fate of whiting particles: calcite growth, partial dissolution, and sedimentation**

419 The end of the whiting season is marked by a decline in calcite mineral abundances in the
420 water column in September (Fig. 3). Although the surface waters of the lake remain supersaturated
421 with respect to calcite in the late summer (Brunskill, 1969), the termination of the whiting may be
422 linked with the decline in abundances of photosynthesizing organisms in shallow waters with time,
423 leading to a shortage of organic surfaces for calcium carbonate heterogeneous nucleation.

424 The duration of the whiting is additionally controlled by the settling rate of mineral
425 particles. Settling rates of mineral grains exponentially increase with size, as shown by Gibbs *et*
426 *al.* (1971). This phenomenon results in a dramatic increase in settling rate as minerals grow longer
427 than 10 μm in length. Based on our assessment of calcite grain sizes, average whiting calcite grains
428 (5-7 μm in length) have a settling rate of ~1 m/day in still waters (based on calculations from Gibbs
429 *et al.*, 1971). Particles likely have somewhat longer residence times in the turbulent mixolimnion
430 than these still-water settling rates imply, and smaller particles likely remain suspended in the
431 upper portion of the lake for longer, contributing to the light scattering by carbonate grains, giving
432 the lake its turquoise color. However, minerals in the mixolimnion likely grow quite fast (up to 2
433 μm/day, based on saturation state rate studies conducted by Wolthers *et al.*, 2012), sinking faster
434 as they grow, and ultimately fall out of the water column, settling in the sediments. Thus, a mineral
435 can quickly grow to 5-7 μm in length over the span of 2-3 days, sinking as it grows. A mineral 1
436 μm in size at the surface will sink <0.5 m in a day but grow to a size of 3 μm over the same span
437 of time. Small minerals, on the order of <5 μm in size, are not found suspended in the water
438 column, likely because the growth rate of these grains is fast following nucleation on organic
439 templates. Minerals larger than 15 μm were not found suspended in the water column, consistent
440 with their calculated very short residence time. All told, the residence time of a mineral grain in

441 the upper 10 m of the lake is estimated to be less than 7 days when taking into account combined
442 growth and sinking. As demonstrated above, calcite particles are furthermore frequently found in
443 aggregates formed by diatom frustules and EPS, which would also increase settling rates. In order
444 to support the continued growth and settling of mineral grains, nucleation of new minerals must
445 be continuous throughout the duration of the whiting event.

446 Abundance of calcite grains in the FGL sediments (Figs. 10, S5, S6) suggests that settling
447 whiting particles reach the bottom of the lake despite some dissolution in the mixolimnion in the
448 late summer (as evidenced by corroded grain surfaces below ~8 m depth in August and September;
449 Figs. 2, 3, S1). Calcite dissolution below ~8 m is explained by the development of slightly
450 understaturated conditions (Havig *et al.*, 2015), possibly due to cumulative respiratory CO_2 build-
451 up through the summer. The sedimented calcite particles display similar shapes and sizes to those
452 found in the water column, but they are slightly more crystalline (Fig. 8b). Calcite in the sediments
453 is found in association with diatom frustules and organic materials, which can be coated by
454 important amounts of calcium (Fig. 8a), reflecting the higher concentrations of dissolved Ca^{2+} in
455 the lake monimolimnion (Havig *et al.*, 2015). Calcite grains and diatoms are the main components
456 of FGL bottom sediments, confirming previous studies, and suggesting that these sediments record
457 biogeochemical signals (such as carbon isotopic signatures) from the lake surface waters (Havig
458 *et al.*, 2017).

5. CONCLUSION

This microscopy study of the annual whiting at Fayetteville Green Lake highlights the role of photosynthetic microorganisms (cyanobacteria and diatoms) and their exuded polymers (EPS) in calcite mineralization through nucleation of an ACC precursor phase. This work describes a previously overlooked role of diatoms and their EPS in calcite precipitation, a mechanism that may be relevant to different types of environments experiencing whiting events.

6. ACKNOWLEDGMENTS

This work was funded through the Penn State Energy and Environmental Sustainability Laboratories (EESL) Green Program and Pennsylvania Space Grant Consortium awards to Chloe Stanton. The authors are indebted to the staff at Green Lakes State Park (NY) for their assistance. Karim Benzerara (Sorbonne Université, CNRS) is thanked for sharing XANES reference spectra, and Stephen Romaniello (University of Tennessee, Knoxville) is thanked for providing a FGL sediment trap sample.

Part of the research described in this paper was performed at the Canadian Light Source, a national research facility of the University of Saskatchewan, which is supported by the Canada Foundation for Innovation (CFI), the Natural Sciences and Engineering Research Council (NSERC), the National Research Council (NRC), the Canadian Institutes of Health Research (CIHR), the Government of Saskatchewan, and the University of Saskatchewan. This research used resources of the Advanced Light Source, a U.S. DOE Office of Science User Facility under contract no. DE-AC02-05CH11231.

7. REFERENCES

Bathurst RGC (1966) Boring algae, micrite envelopes and lithification of molluscan biosparites. *Geological Journal* **5**, 15–32.

Benzerara K, Bolzoni R, Monteil C, Beyssac O, Forni O, Alonso B, Asta MP, Lefevre C (2021) The gammaproteobacterium Achromatium forms intracellular amorphous calcium carbonate and not (crystalline) calcite. *Geobiology* **19**, 199–213.

Benzerara K, Skouri-Panet F, Li J, Ferard C, Gugger M, Laurent T, Couradeau E, Ragon M, Cosmidis J, Menguy N, Margaret-Oliver I, Tavera R, Lopez-Garcia P, Moreira D (2014) Intracellular Ca-carbonate biomineralization is widespread in cyanobacteria. *Proceedings of the National Academy of Sciences* **111**, 10933–10938.

Benzerara K, Yoon TH, Tyliszczak T, Constantz B, Spormann AM, Brown GE (2004) Scanning transmission X-ray microscopy study of microbial calcification. *Geobiology* **2**, 249–259.

Beveridge TJ (1981) Ultrastructure, Chemistry, and Function of the Bacterial Wall. In: *International Review of Cytology* (eds. Bourne GH, Danielli JF, Jeon KW). Academic Press, pp. 229–317.

Boss SK, Neumann A (1993) Physical versus chemical processes of "whiting" formation in the Bahamas. *Carbonates and Evaporites*.

Brandes JA, Wirick S, Jacobsen C (2010) Carbon *K* -edge spectra of carbonate minerals. *Journal of Synchrotron Radiation* **17**, 676–682.

Broecker W (2012) Section 9. Whitings. *Geochemical Perspectives* **1**, 249–250.

Broecker WS, Sanyal A, Takahashi T (2000) The origin of Bahamian Whitings revisited. *Geophysical Research Letters* **27**, 3759–3760.

Broecker WS, Takahashi T (1966) Calcium carbonate precipitation on the Bahama Banks. *Journal of Geophysical Research (1896-1977)* **71**, 1575–1602.

Brunskill GJ (1969) Fayetteville Green Lake, New York. II. Precipitation and Sedimentation of Calcite in a Meromictic Lake with Laminated Sediments. *Limnology and Oceanography* **14**, 830–847.

Cam N, Georgelin T, Jaber M, Lambert J-F, Benzerara K (2015) In vitro synthesis of amorphous Mg-, Ca-, Sr- and Ba-carbonates: What do we learn about intracellular calcification by cyanobacteria? *Geochimica et Cosmochimica Acta* **161**, 36–49.

Chan CS, Fakra SC, Edwards DC, Emerson D, Banfield JF (2009) Iron oxyhydroxide mineralization on microbial extracellular polysaccharides. *Geochimica et Cosmochimica Acta* **73**, 3807–3818.

Chan CS, Fakra SC, Emerson D, Fleming EJ, Edwards KJ (2011) Lithotrophic iron-oxidizing bacteria produce organic stalks to control mineral growth: implications for biosignature formation. *The ISME Journal* **5**, 717–727.

Chen X, Romaniello SJ, Anbar AD (2021) Preliminary exploration of molybdenum isotope fractionation during coprecipitation of molybdate with abiotic and microbial calcite. *Chemical Geology* **566**, 120102.

Cosmidis J, Benzerara K (2014) Soft X-ray Scanning Transmission Spectromicroscopy. In: *Biomineralization Sourcebook: Characterization of Biominerals and Biomimetic Materials*. E. DiMasi and L.B. Gower, London, UK, pp. 115–133.

Cosmidis J, Benzerara K, Guyot F, Skouri-Panet F, Duprat E, Férard C, Guigner J-M, Babonneau F, Coelho C (2015a) Calcium-Phosphate Biomineralization Induced by Alkaline

Phosphatase Activity in Escherichia coli: Localization, Kinetics, and Potential Signatures in the Fossil Record. *Frontiers in Earth Science* **3**.
Cosmidis J, Benzerara K, Nassif N, Tyliszczak T, Bourdelle F (2015b) Characterization of Ca-phosphate biological materials by scanning transmission X-ray microscopy (STXM) at the Ca L2,3-, P L2,3- and C K-edges. *Acta Biomaterialia* **12**, 260–269.
Culver DA, Brunskill GJ (1969) Fayetteville Green Lake, New York. V. Studies of primary production and zooplankton in a meromictic marl lake: primary production in Green Lake. *Limnology and Oceanography* **14**, 862–873.
DeMott LM, Napieralski SA, Junium CK, Teece M, Scholz CA (2020) Microbially influenced lacustrine carbonates: A comparison of Late Quaternary Lahontan tufa and modern thrombolite from Fayetteville Green Lake, NY. *Geobiology* **18**, 93–112.
Dierssen HM, Zimmerman RC, Burdige DJ (2009) Optics and remote sensing of Bahamian carbonate sediment whitings and potential relationship to wind-driven Langmuir circulation. *Biogeosciences* **6**, 487–500.
Dittrich M, Kurz P, Wehrli B (2004) The Role of Autotrophic Picocyanobacteria in Calcite Precipitation in an Oligotrophic Lake. *Geomicrobiology Journal* **21**, 45–53.
Dittrich M, Obst M (2004) Are Picoplankton Responsible for Calcite Precipitation in Lakes? *AMBIO: A Journal of the Human Environment* **33**, 559–564.
Dupraz C, Reid RP, Braissant O, Decho AW, Norman RS, Visscher PT (2009) Processes of carbonate precipitation in modern microbial mats. *Earth-Science Reviews* **96**, 141–162.
Dupraz C, Visscher PT (2005) Microbial lithification in marine stromatolites and hypersaline mats. *Trends in Microbiology* **13**, 429–438.
Ehrlich H (2010) Chitin and collagen as universal and alternative templates in biomineralization. *International Geology Review* **52**, 661–699.
Ehrlich H, Motylenko M, Sundareshwar PV, Ereskovsky A, Zgłobicka I, Noga T, Płociński T, Tsurkan MV, Wyroba E, Suski S, Bilski H, Wysokowski M, Stöcker H, Makarova A, Vyalikh D, Walter J, Molodtsov SL, Bazhenov VV, Petrenko I, Langer E, Richter A, Niederschlag E, Pisarek M, Springer A, Gelinsky M, Rafaja D, Witkowski A, Meyer DC, Jesionowski T, Kurzydłowski KJ (2016) Multiphase Biomineralization: Enigmatic Invasive Siliceous Diatoms Produce Crystalline Calcite. *Advanced Functional Materials* **26**, 2503–2510.
Enyedi NT, Makk J, Kótai L, Berényi B, Klébert S, Sebestyén Z, Molnár Z, Borsodi AK, Leél-Őssy S, Demény A, Németh P (2020) Cave bacteria-induced amorphous calcium carbonate formation. *Scientific Reports* **10**, 8696.
Fuchs A, Selmeczy GB, Kasprzak P, Padisák J, Casper P (2016) Coincidence of sedimentation peaks with diatom blooms, wind, and calcite precipitation measured in high resolution by a multi-trap. *Hydrobiologia* **763**, 329–344.
Fulton JM, Arthur MA, Thomas B, Freeman KH (2018) Pigment carbon and nitrogen isotopic signatures in euxinic basins. *Geobiology* **16**, 429–445.
Gibbs RJ, Matthews MD, Link DA (1971) The relationship between sphere size and settling velocity. *Journal of Sedimentary Research* **41**, 7–18.
Gomez FJ, Mlewski C, Boidi FJ, Farías ME, Gérard E (2018) Calcium Carbonate Precipitation in Diatom-rich Microbial Mats: The Laguna Negra Hypersaline Lake, Catamarca, Argentina. *Journal of Sedimentary Research* **88**, 727–742.

566 Gügi B, Le Costaouec T, Burel C, Lerouge P, Helbert W, Bardor M (2015) Diatom-Specific
567 Oligosaccharide and Polysaccharide Structures Help to Unravel Biosynthetic Capabilities in
568 Diatoms. *Marine Drugs* **13**, 5993–6018.
569 Havig JR, Hamilton TL, McCormick M, McClure B, Sowers T, Wegter B, Kump LR (2017)
570 Water column and sediment stable carbon isotope biogeochemistry of permanently redox-
571 stratified Fayetteville Green Lake, New York, U.S.A.: Carbon isotopes at FGL. *Limnology and*
572 *Oceanography*.
573 Havig JR, McCormick ML, Hamilton TL, Kump LR (2015) The behavior of biologically
574 important trace elements across the oxic/euxinic transition of meromictic Fayetteville Green
575 Lake, New York, USA. *Geochimica et Cosmochimica Acta* **165**, 389–406.
576 Herth W, Barthlott W (1979) The site of β-chitin fibril formation in centric diatoms. I. Pores and
577 fibril formation. *Journal of Ultrastructure Research* **68**, 6–15.
578 Hitchcock A (2012) aXis 2000 - Analysis of X-ray Images and Spectra.
579 Hodell DA, Schelske CL, Fahnenstiel GL, Robbins LL (1998) Biologically induced calcite and
580 its isotopic composition in Lake Ontario. *Limnology and Oceanography* **43**, 187–199.
581 Hunter SE (2012) *Spatio-temporal Variability in the Phototrophic Chemocline Community at*
582 *Fayetteville Green Lake (new York)* (Master Thesis).
583 Kamennaya NA, Hu P, Jansson C (2020) Sedimentation of ballasted cells-free EPS in
584 meromictic Fayetteville Green Lake. *Geobiology* **18**, 80–92.
585 Kirkwood AE, Shea T, Jackson LJ, McCauley E (2007) Didymosphenia geminata in two Alberta
586 headwater rivers: an emerging invasive species that challenges conventional views on algal
587 bloom development. *Canadian Journal of Fisheries and Aquatic Sciences* **64**, 1703–1709.
588 Küchler-Krischun J, Kleiner J (1990) Heterogeneously nucleated calcite precipitation in Lake
589 Constance. A short time resolution study. *Aquatic Sciences* **52**, 176–197.
590 Lawrence JR, Swerhone GDW, Leppard GG, Araki T, Zhang X, West MM, Hitchcock AP
591 (2003) Scanning Transmission X-Ray, Laser Scanning, and Transmission Electron Microscopy
592 Mapping of the Exopolymeric Matrix of Microbial Biofilms. *Applied and Environmental*
593 *Microbiology* **69**, 5543–5554.
594 Lehmann J, Solomon D, Brandes J, Fleckenstein H, Jacobson C, Thieme J (2009) Synchrotron-
595 Based Near-Edge X-Ray Spectroscopy of Natural Organic Matter in Soils and Sediments. In:
596 *Biophysico-Chemical Processes Involving Natural Nonliving Organic Matter in Environmental*
597 *Systems* (eds. Senesi N, Xing B, Huang PM). John Wiley & Sons, Inc., Hoboken, NJ, USA, pp.
598 729–781.
599 Lisle JT, Robbins LL (2016) Viral Lysis of Photosynthesizing Microbes As a Mechanism for
600 Calcium Carbonate Nucleation in Seawater. *Frontiers in Microbiology* **7**.
601 Long JS, Hu C, Robbins LL, Byrne RH, Paul JH, Wolny JL (2017) Optical and biochemical
602 properties of a southwest Florida whiting event. *Estuarine, Coastal and Shelf Science* **196**, 258–
603 268.
604 Martignier A, Pacton M, Filella M, Jaquet J-M, Barja F, Pollok K, Langenhorst F, Lavigne S,
605 Guagliardo P, Kilburn MR, Thomas C, Martini R, Ariztegui D (2017) Intracellular amorphous
606 carbonates uncover a new biomineralization process in eukaryotes. *Geobiology* **15**, 240–253.
607 Metzler R, Zhou D, Abrecht M, Chiou J-W, Guo J, Ariosa D, Coppersmith S, Gilbert P (2008)
608 Polarization-dependent imaging contrast in abalone shells. *Physical Review B* **77**.

Meyer KM, Macalady JL, Fulton JM, Kump LR, Schaperdoth I, Freeman KH (2011) Carotenoid biomarkers as an imperfect reflection of the anoxygenic phototrophic community in meromictic Fayetteville Green Lake. *Geobiology* **9**, 321–329.
Mitsunobu S, Zhu M, Takeichi Y, Ohigashi T, Suga H, Makita H, Sakata M, Ono K, Mase K, Takahashi Y (2014) Nanoscale Identification of Extracellular Organic Substances at the Microbe–Mineral Interface by Scanning Transmission X-ray Microscopy. *Chemistry Letters* **44**, 91–93.
Monteil CL, Benzerara K, Menguy N, Bidaud CC, Michot-Achdjian E, Bolzoni R, Mathon FP, Coutaud M, Alonso B, Garau C, Jézéquel D, Viollier E, Ginet N, Floriani M, Swaraj S, Sachse M, Busigny V, Duprat E, Guyot F, Lefevre CT (2021) Intracellular amorphous Ca-carbonate and magnetite biomineralization by a magnetotactic bacterium affiliated to the Alphaproteobacteria. *The ISME Journal* **15**, 1–18.
Morse JW, Gledhill DK, Millero FJ (2003) CaCO3 precipitation kinetics in waters from the great Bahama bank:: Implications for the relationship between bank hydrochemistry and whitings. *Geochimica et Cosmochimica Acta* **67**, 2819–2826.
Novis P, Schallenberg M, Saulnier-Talbot É, Kilroy C, Reid M (2017) The diatom Lindavia intermedia identified as the producer of nuisance pelagic mucilage in lakes. *New Zealand Journal of Botany* **55**, 479–495.
Oduro H, Kamyshny A, Zerkle AL, Li Y, Farquhar J (2013) Quadruple sulfur isotope constraints on the origin and cycling of volatile organic sulfur compounds in a stratified sulfidic lake. *Geochimica et Cosmochimica Acta* **120**, 251–262.
Politi Y, Metzler RA, Abrecht M, Gilbert B, Wilt FH, Sagi I, Addadi L, Weiner S, Gilbert PUPA (2008) Transformation mechanism of amorphous calcium carbonate into calcite in the sea urchin larval spicule. *Proceedings of the National Academy of Sciences* **105**, 17362–17366.
Purkis S, Cavalcante G, Rohtla L, Oehlert AM, Harris P (Mitch), Swart PK (2017) Hydrodynamic control of whitings on Great Bahama Bank. *Geology* **45**, 939–942.
Robbins LL, Blackwelder PL (1992) Biochemical and ultrastructural evidence for the origin of whitings: A biologically induced calcium carbonate precipitation mechanism. *Geology* **20**, 464.
Robbins LL, Tao Y, Evans CA (1997) Temporal and spatial distribution of whitings on Great Bahama Bank and a new lime mud budget. *Geology* **25**, 947–950.
Rojas CA, Torio ADS, Park S, Bosak T, Klepac-Ceraj V (2021) Organic electron donors and terminal electron acceptors structure anaerobic microbial communities and interactions in a permanently stratified sulfidic lake. *bioRxiv* 2021.02.16.431432.
Schultze-Lam S, Harauz G, Beveridge TJ (1992) Participation of a cyanobacterial S layer in fine-grain mineral formation. *Journal of Bacteriology* **174**, 7971–7981.
Schultze-Lam S, Schultze-Lam S, Beveridge TJ, Des Marais DJ (1997) Whiting events: Biogenic origin due to the photosynthetic activity of cyanobacterial picoplankton. *Limnology and Oceanography* **42**, 133–141.
Shinn EA, Steinen RP, Lidz BH, Swart PK (1989) Whitings, a sedimentologic dilemma. *Journal of Sedimentary Research* **59**, 147–161.
Shiraishi F, Omori T, Tomioka N, Motai S, Suga H, Takahashi Y (2020) Characteristics of CaCO3 nucleated around cyanobacteria: Implications for calcification process. *Geochimica et Cosmochimica Acta* **285**, 55–69.
Shnyukova EI, Zolotareva EK (2015) Diatom Exopolysaccharides: a Review. *International Journal on Algae* **17**.

Stabel H-H (1986) Calcite precipitation in Lake Constance: Chemical equilibrium, sedimentation, and nucleation by algae1. *Limnology and Oceanography* **31**, 1081–1094.
Svetličić V, Žutić V, Pletikapić G, Radić TM (2013) Marine Polysaccharide Networks and Diatoms at the Nanometric Scale. *International Journal of Molecular Sciences* **14**, 20064–20078.
Swart PK, Oehlert AM, Mackenzie GJ, Eberli GP, Reijmer JJG (2014) The fertilization of the Bahamas by Saharan dust: A trigger for carbonate precipitation? *Geology* **42**, 671–674.
Takahashi T, Broecker W, Li YH, Thurber D (1968) Chemical and Isotopic Balances for a Meromictic Lake. *Limnology and Oceanography* **13**, 272–292.
Thompson JB (2000) Microbial Whitings. In: *Microbial Sediments*. Springer, Berlin, Heidelberg, pp. 250–260.
Thompson JB, Ferris FG (1990) Cyanobacterial precipitation of gypsum, calcite, and magnesite from natural alkaline lake water. *Geology* **18**, 995.
Thompson JB, Ferris FG, Smith DA (1990) Geomicrobiology and Sedimentology of the Mixolimnion and Chemocline in Fayetteville Green Lake, New York. *PALAIOS* **5**, 52–75.
Urbani R, Sist P, Pletikapić G, Radić TM, Svetličić V, Žutic V (2012) Diatom Polysaccharides: Extracellular Production, Isolation and Molecular Characterization. *The Complex World of Polysaccharides*.
Weiner S, Sagi I, Addadi L (2005) Choosing the Crystallization Path Less Traveled. *Science* **309**, 1027–1028.
Winsborough BM (2000) Diatoms and Benthic Microbial Carbonates. In: *Microbial Sediments* (eds. Riding RE, Awramik SM). Springer, Berlin, Heidelberg, pp. 76–83.
Winsborough BM, Golubić S (1987) The Role of Diatoms in Stromatolite Growth: Two Examples from Modern Freshwater Settings1. *Journal of Phycology* **23**, 195–201.
Wolthers M, Nehrke G, Gustafsson JP, Van Cappellen P (2012) Calcite growth kinetics: Modeling the effect of solution stoichiometry. *Geochimica et Cosmochimica Acta* **77**, 121–134.
Zerkle AL, Kamyshny A, Kump LR, Farquhar J, Oduro H, Arthur MA (2010) Sulfur cycling in a stratified euxinic lake with moderately high sulfate: Constraints from quadruple S isotopes. *Geochimica et Cosmochimica Acta* **74**, 4953–4970.
Zhu T, Dittrich M (2016) Carbonate Precipitation through Microbial Activities in Natural Environment, and Their Potential in Biotechnology: A Review. *Frontiers in Bioengineering and Biotechnology* **4**.

8. FIGURES AND CAPTIONS

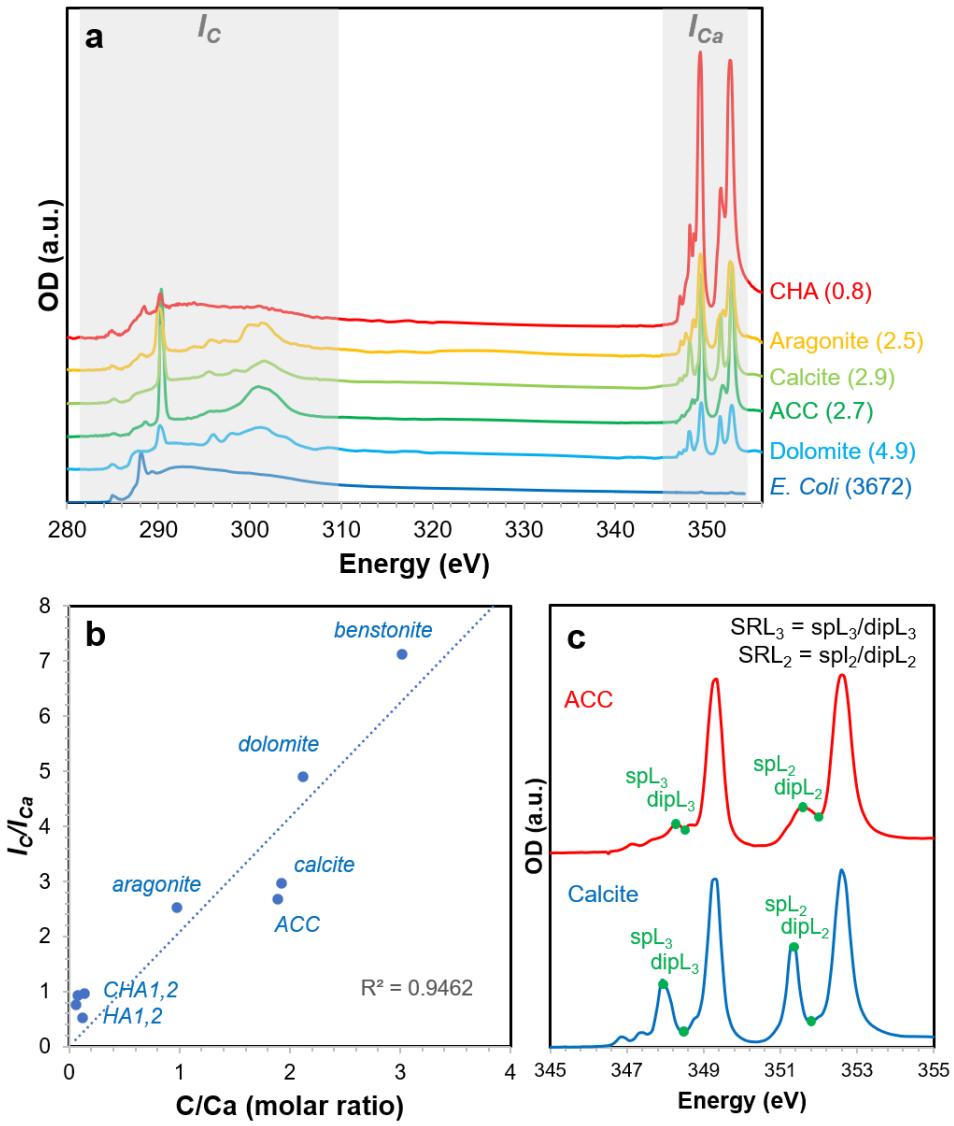

Figure 1. STXM methods for the calculation of I_C/I_{Ca} ratios and splitting ratios (SRL_2 and SRL_3). (a) XANES spectra of several reference compounds spanning the C K- and Ca $L_{2,3}$-edges, and calculated I_C/I_{Ca} ratios. I_C/I_{Ca} is calculated as the ratio of the areas under the curve in the 280-310 eV region versus the 345-354 eV region (shaded areas). Calculated I_C/I_{Ca} ratios are noted (numbers in brackets). The C K-edge spectra of carbonate minerals typically display strong absorption peaks at 290.3 eV and broad absorption bands around 301.5 eV. Some of the mineral

694 references contain minor amounts of organics, detectable as small peaks in the 285.0-288.7 eV
695 region. ACC: amorphous calcium carbonate; CHA: carbonated hydroxyapatite (francolite). (b)
696 Plot showing the correlation between I_C/I_{Ca} ratios and measured C/Ca molar ratios for different
697 calcium-bearing reference minerals. ACC: amorphous calcium carbonate; CHA: carbonated
698 hydroxyapatite (francolite), HA: hydroxyapatite. (c) Ca $L_{2,3}$-edge spectra of a reference calcite
699 and amorphous calcium carbonate, showing the method for the calculation of splitting ratios,
700 quantifying calcium carbonate crystallinity (see Politi et al., 2008).
701
702

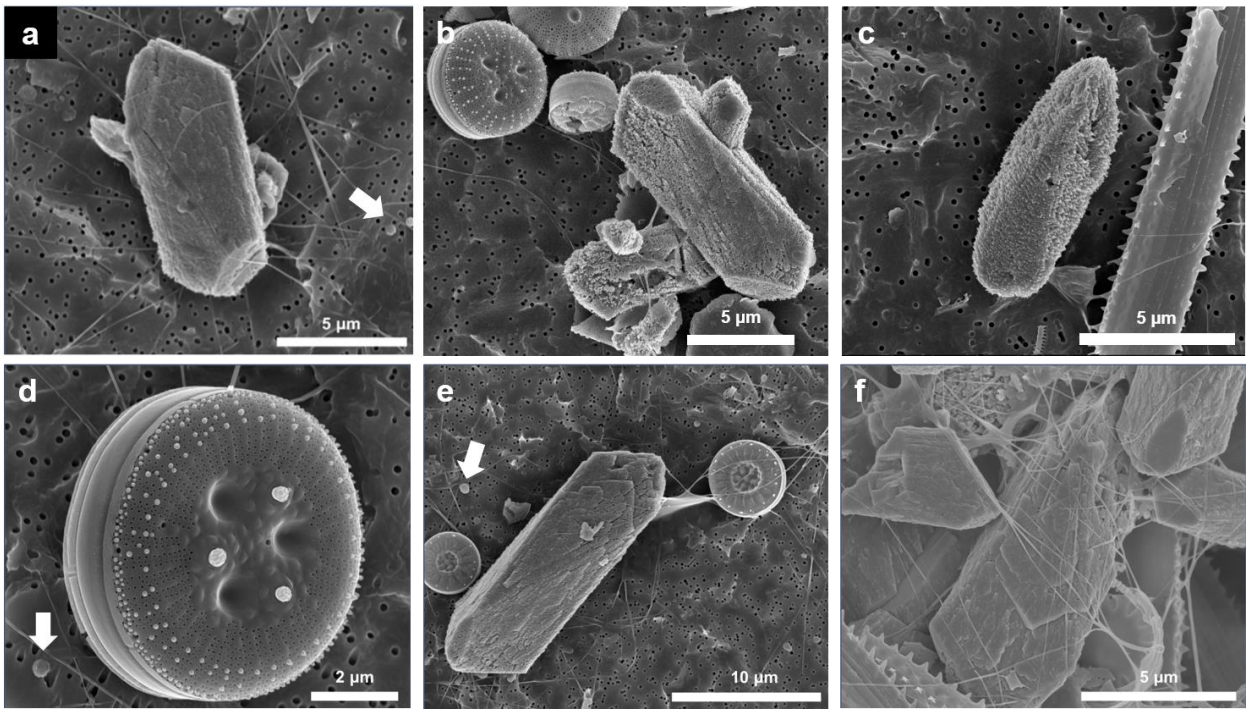

Figure 2. SEM images of whiting particles from the FGL water column. (a) Smooth-surfaced calcium carbonate mineral interlaid with organic fibrils, characteristic of peak whiting (3 m depth, June). (b) Pitted calcium carbonate grains and centric diatoms (8 m depth, August). (c) Increasingly pitted and rounded carbonate grain, along a with pennate diatom (8 m depth, September 8). (d) A centric diatom with organic material (EPS) extruding from the valve pores (3 m depth, June 30). The brightness of the extruding material is indicative of heavy elements associated with the EPS (possibly adsorbed ions). (e) A centric diatom, attached to a carbonate mineral grain with organic fibrils (3 m depth, June). (e) Sediment trap whiting material (July 2017, 13 m depth) showing carbonate minerals within a dense mesh of organic fibrils. White arrows in (a), (d), and (e) point to possible microbial cells (*Synechococcus*).

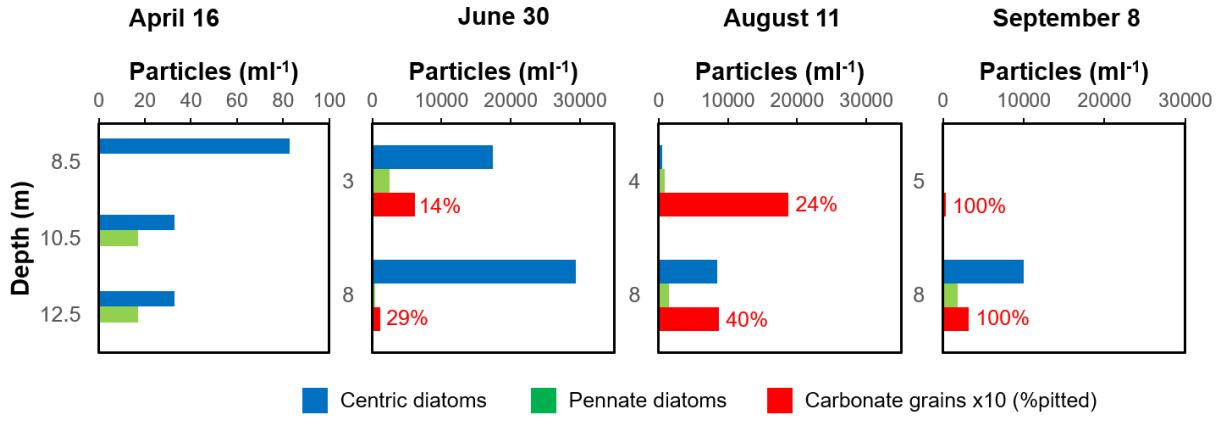

714

715 **Figure 3.** Particle types and abundances at different depths in the water column of FGL before
716 and throughout the whiting season, as counted from SEM images. Note that abundances of
717 carbonate grains have been divided by ten, and that sample collection depth vary for different
718 sampling times. The percentage of pitted carbonate particles (relative to smooth grains) is
719 indicated (brackets).

720

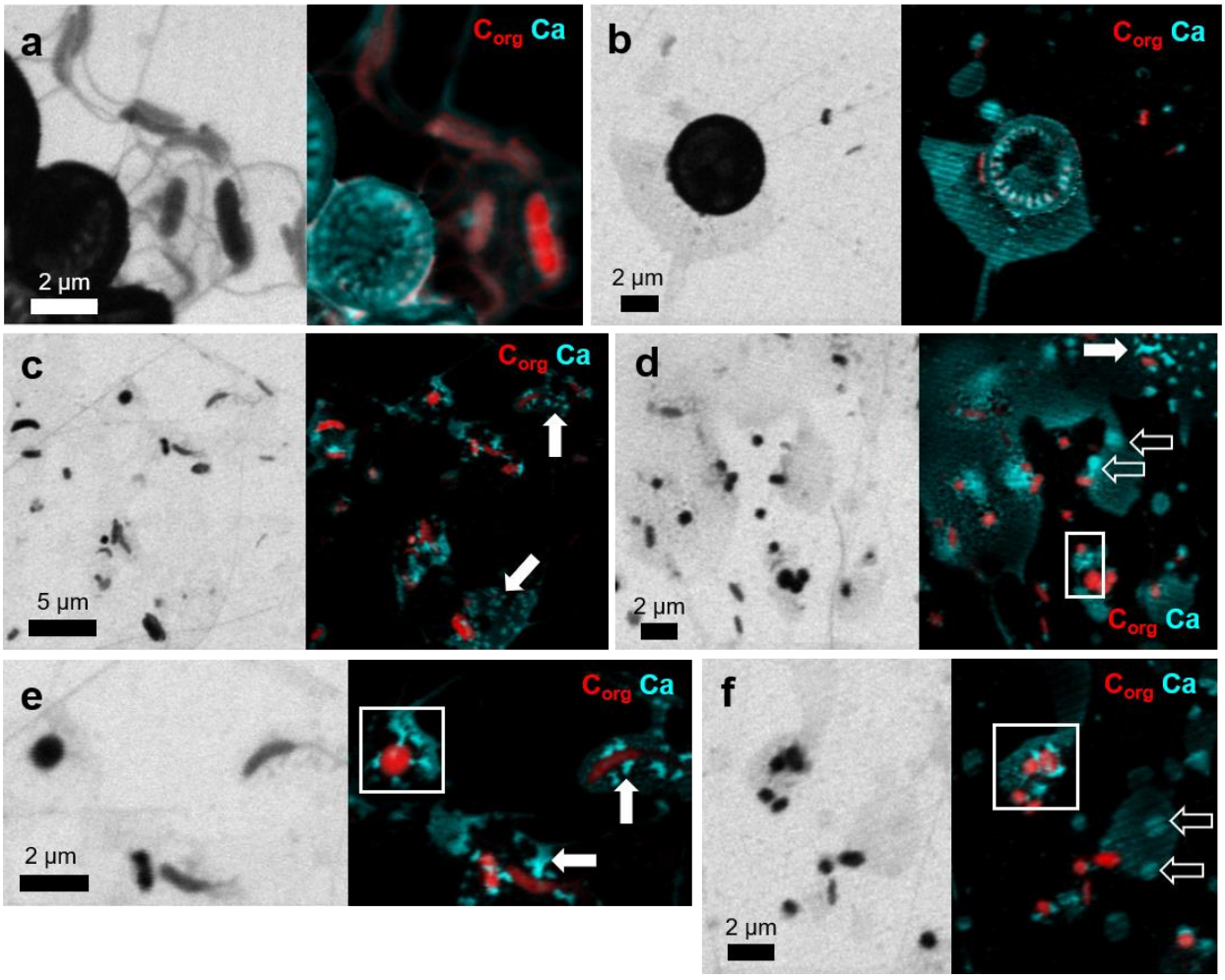

721

722 **Figure 4.** STXM analyses of pre-whiting particles from the FGL water column (April, 8 m
723 depth). Images (left) were acquired at 288.2 eV. The corresponding maps (right) show the
724 distribution of organic carbon (red) and calcium (cyan). Whites squares show the locations of the
725 image stacks displayed in Fig. S3 and Fig. 7. White arrows show the location of irregularly
726 shaped calcium-rich clots within EPS films (identified as ACC minerals), while open arrows
727 show micron-scale, round calcium enrichments that may correspond to Ca^{2+} adsorbed on empty
728 EPS envelopes of *Synechococcus* cells. Note that EPS films and fibrils visible on STXM images
729 do not appear on organic carbon maps, which may be due to excessive thinness (see main text).

730

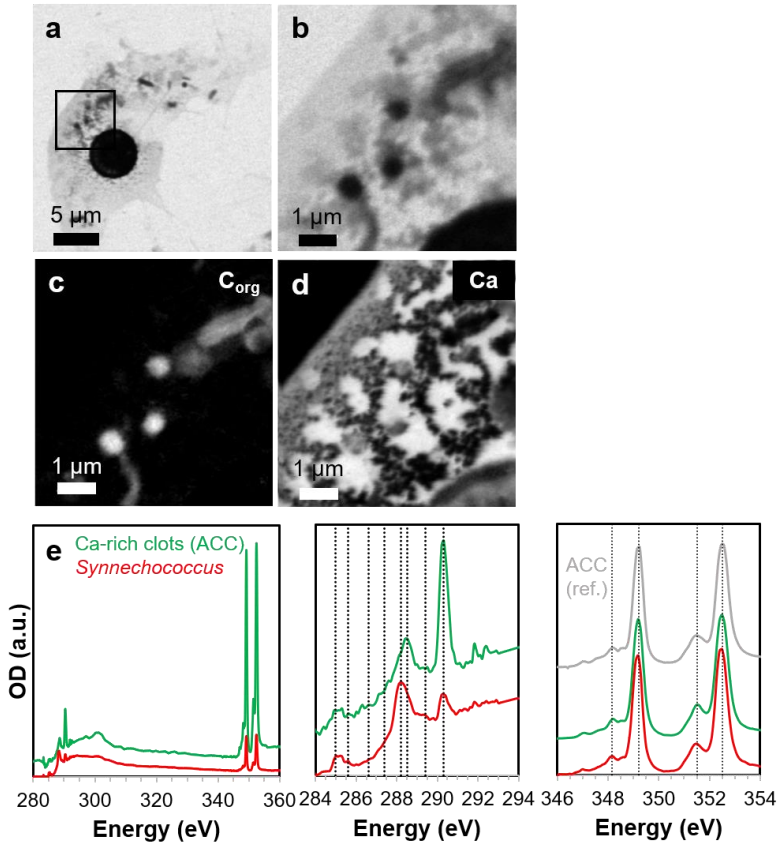

731

732 **Figure 5.** STXM analyses of diatom EPS and *Synechococcus* cells from a FGL pre-whiting
733 sample (April, 8 m depth). (a) Image obtained at 288.2 eV. A centric diatom, surrounded by EPS
734 film, is visible. (b) Close-up on the area depicted by a square in (a). *Synechococcus* cells are
735 present within the EPS film. (c) Organic carbon map. (d) Calcium map. (e) XANES spectra
736 representative of calcium-rich clots within the EPS film (green) and *Synechococcus* cells (red). C
737 K-edge spectra (middle panel): vertical lines correspond to the absorption energies of different
738 functional groups (see main text). Ca $L_{2,3}$-edge spectra (right panel): vertical lines correspond to
739 the position of the main peaks in the reference amorphous calcium carbonate (ACC) spectrum
740 (grey). The calcium-rich clots are identified as calcium-carbonate phases based on the presence
741 of strong X-ray absorption at 290.3 eV and 301.5 eV. Their calculated splitting ratios are SRL_3 ~
742 1.2 and SRL_2 ~ 1.3, corresponding to ACC.

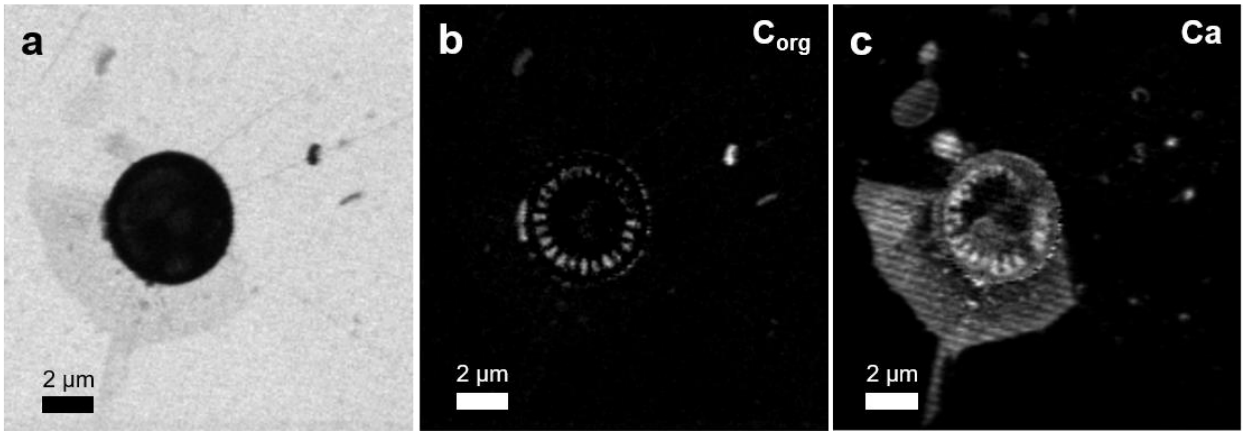

Figure 6. STXM image and maps of a centric diatom and associated EPS in a FGL pre-whiting sample (April, 8 m depth). (a) Image at 288.2 eV. (b) Organic carbon map. (c) Calcium map. Calcium is particularly enriched on the EPS material around the diatom, and on the perforations of the frustule (from which EPS are typically exuded).

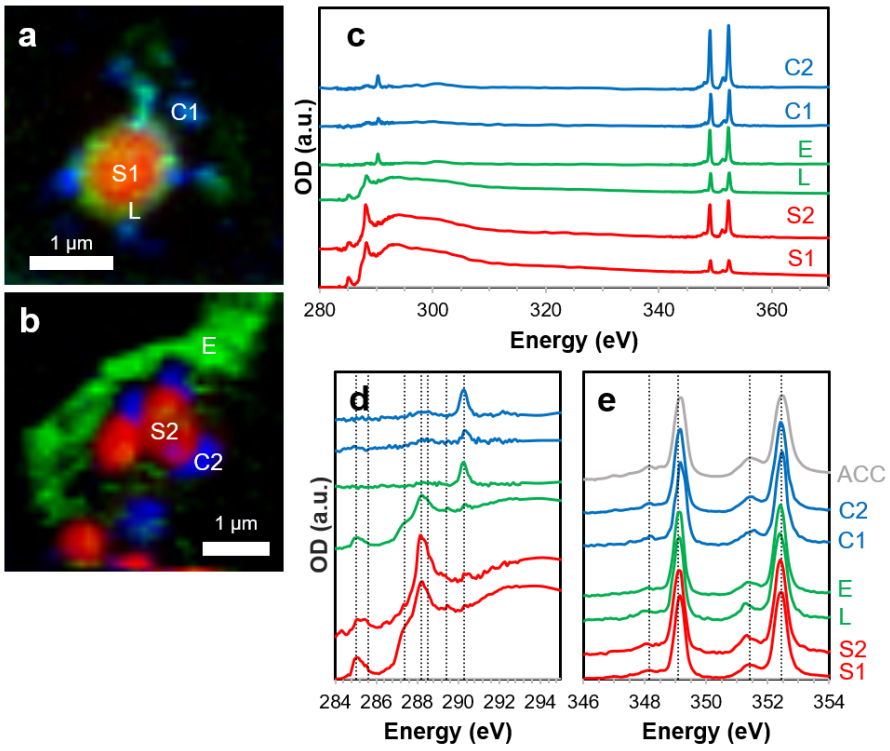

Figure 7. STXM analyses of *Synechococcus* cells, EPS and calcium-rich grains in a FGL pre-whiting sample (April, 8 m depth). (a) and (b): maps showing the distribution of different components extracted from image stacks. S1, S2: *Synechococcus* cells; L: outer layer of a cell; E: EPS; C1,C2: calcium-rich grains. (c) Corresponding XANES spectra spanning the C K- and Ca $L_{2,3}$-edges. (d) C K-edge XANES spectra normalized at 320 eV. Vertical lines correspond to energy positions of the main absorption features of different function groups (see main text). (e) Ca $L_{2,3}$-edge spectra, normalized at 349.2 eV (energy of the Ca L_3 peak). Vertical lines correspond to the energy positions of the main absorption features of amorphous calcium carbonate (ACC). Both the calcium-rich grains and EPS have spectroscopic signatures consistent with ACC, showing that ACC is nucleating at the surface of *Synechococcus* cells, and as nano-phases on EPS.

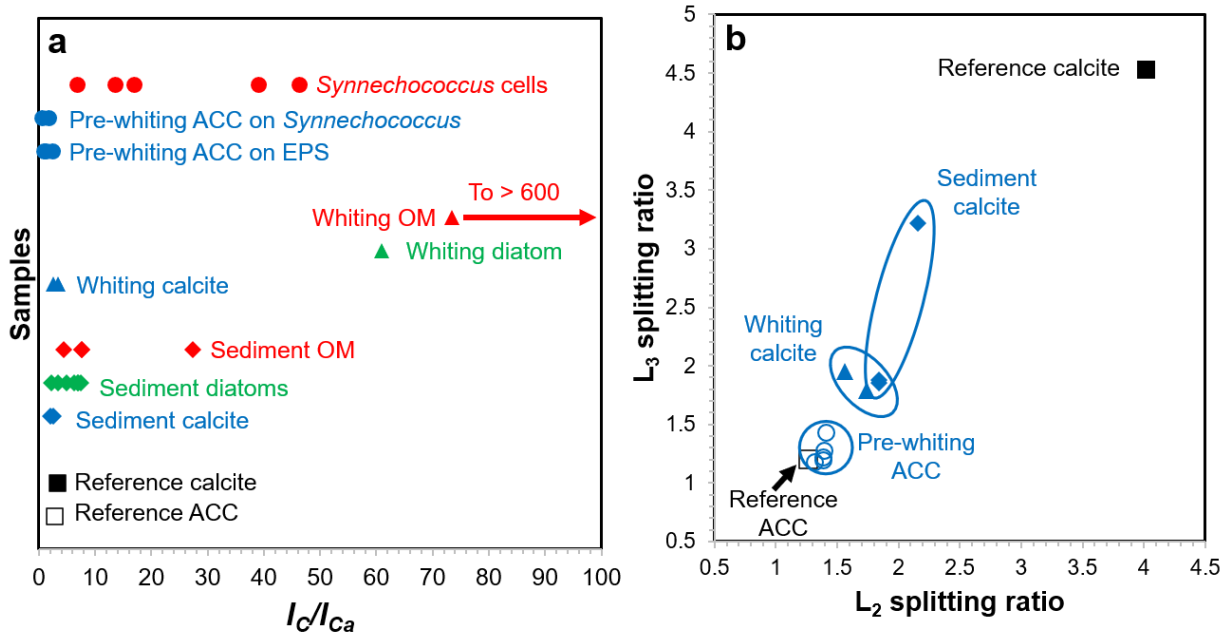

763

764 **Figure 8.** I_C/I_{Ca} ratios and splitting ratios (SRL_3, SRL_2) for different types of samples from the
765 FGL water column and sediment. Ratios calculated from reference spectra for calcite and
766 amorphous calcium carbonate (ACC) are also plotted for comparison. (a) I_C/I_{Ca} ratios: Pre-
767 whiting *Synechococcus* cells and ACC correspond to the water column sample collected in April
768 at 8 m depth. Whiting calcite, diatoms, and organic matter (OM) correspond to sediment trap
769 samples (July, 13.5 m depth). Note that sediment trap OM I_C/I_{Ca} values range from ~73 to > 600
770 (off chart). Sediment calcite, diatoms and OM correspond to sediment core samples. (b) SRL_3
771 versus SRL_2 plot for calcium carbonate particles from the pre-whiting water column (April, 8 m
772 depth) (ACC), the sediment trap (whiting calcite) and the sediment core (sediment calcite). Only
773 particles with I_C/I_{Ca} ratios smaller that 3.3, identified as calcium carbonate minerals, are plotted
774 on this chart.

775

776

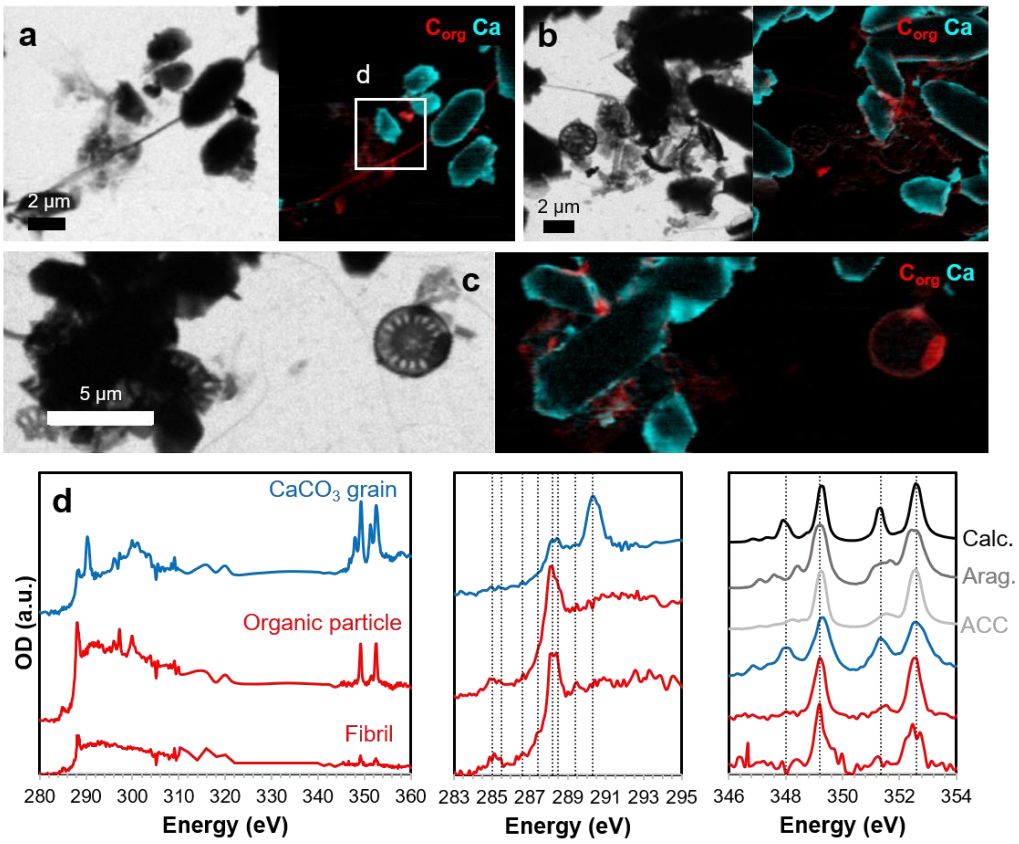

Figure 9. STXM analyses of settling whiting particles collected in a sediment trap (July 2017, 13.5 m depth). (a-c) Images at 288.2 eV (left) and maps of organic carbon (red) and calcium (cyan) (right). The interior of $CaCO_3$ grains sometimes appear black on calcium maps due the excessive thickness of the grains, causing saturation of the X-ray absorption signal. The white box in (a) represents the location of the image stack from which spectra shown in (d) were extracted. (d) XANES spectra representative of a $CaCO_3$ grain, an organic fibril, and a dense organic carbon particle in (a). C K-edge spectra (middle panel): vertical lines correspond to the absorption energies of different functional groups (see main text). Ca $L_{2,3}$-edge spectra (right panel): vertical lines correspond to the position of the main peaks in a reference calcite (Calc.) spectrum (black). Reference Ca $L_{2,3}$-edge XANES spectra for aragonite (Arag.) and amorphous calcium carbonate (ACC) are also shown.

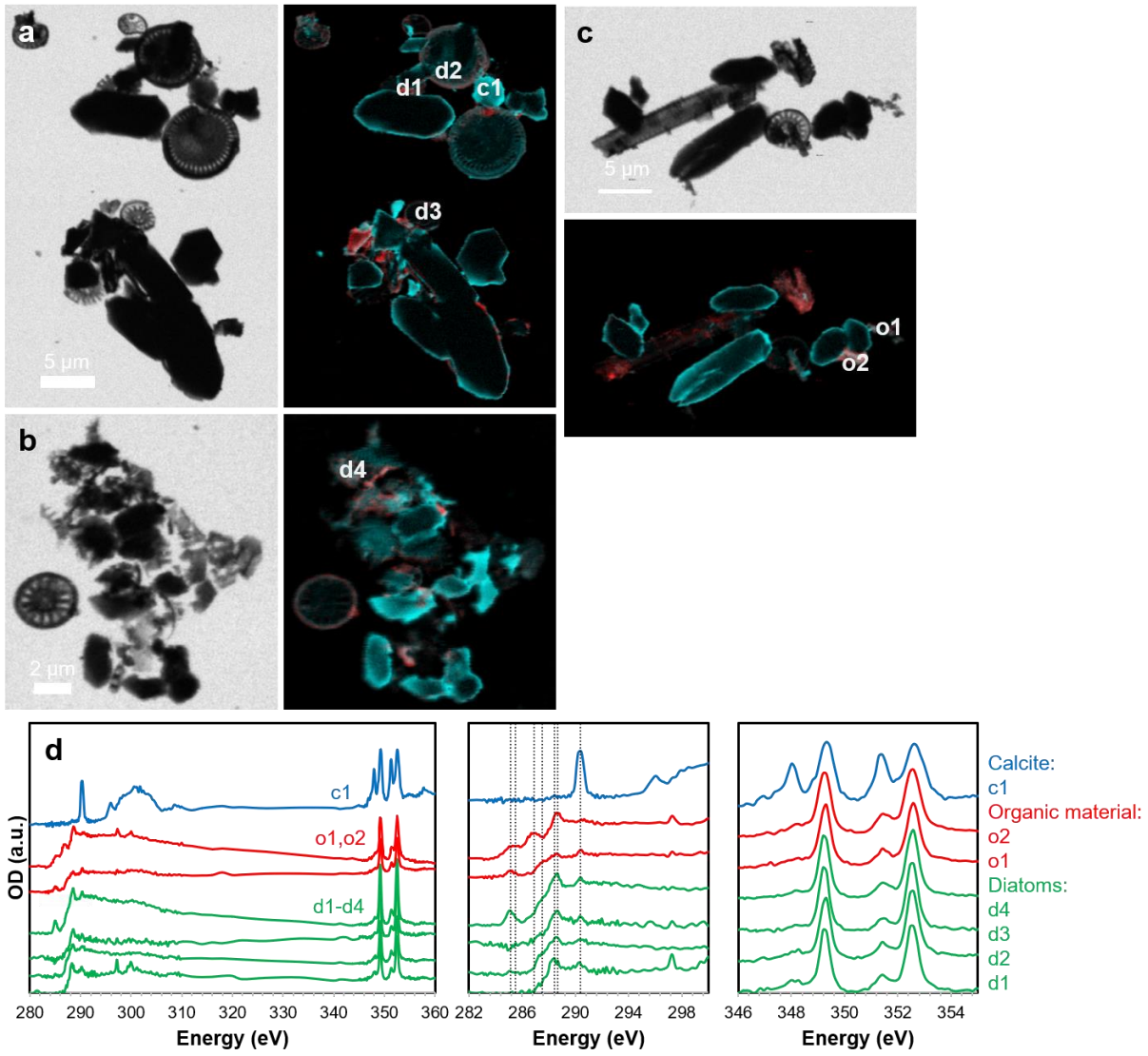

789

790 **Figure 10.** STXM analyses of particles from a FGL sediment core at 0-2 inches (a,b) and 2-4

791 inches (c) depths below the lake floor. (a-c) Images at 288.2 eV (left) and maps of organic

792 carbon (red) and calcium (cyan) (right). The locations from which XANES spectra shown in (d)

793 were extracted are indicated: c1 (calcite grain), o1-o2 (organic material) and d1-d4 (diatoms). (d)

794 Corresponding XANES spectra. C K-edge spectra (middle panel): vertical lines correspond to

795 the absorption energies of different functional groups (see main text). Right panel: Ca $L_{2,3}$-edge

796 spectra.

Supporting Information

A re-examination of the mechanism of whiting events: A new role for diatoms in Fayetteville Green Lake (New York, USA)

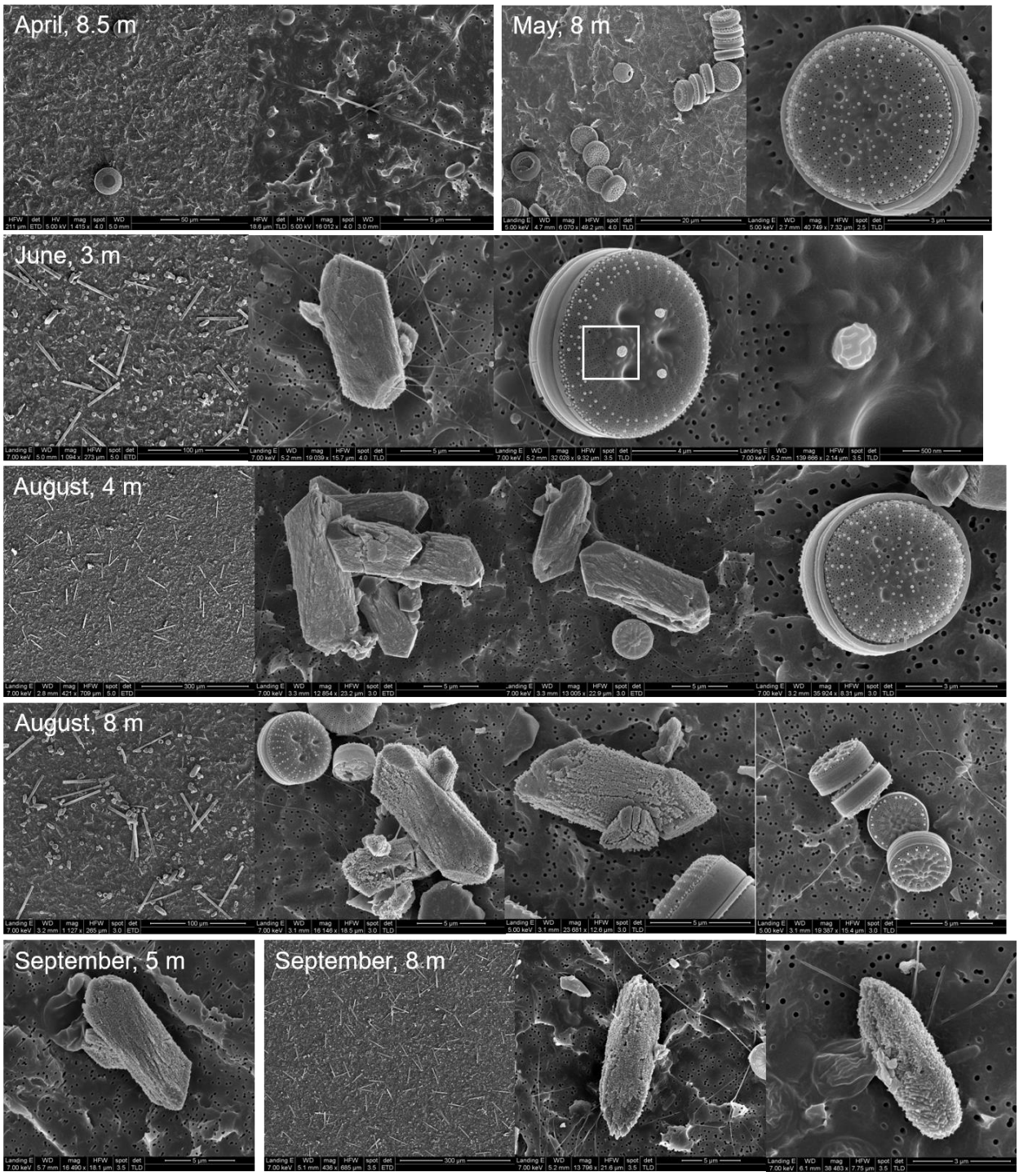

Figure S1. SEM images of FGL water column particulate samples collected on filters throughout the 2018 whiting season. Collection times (months) and depths are indicated.

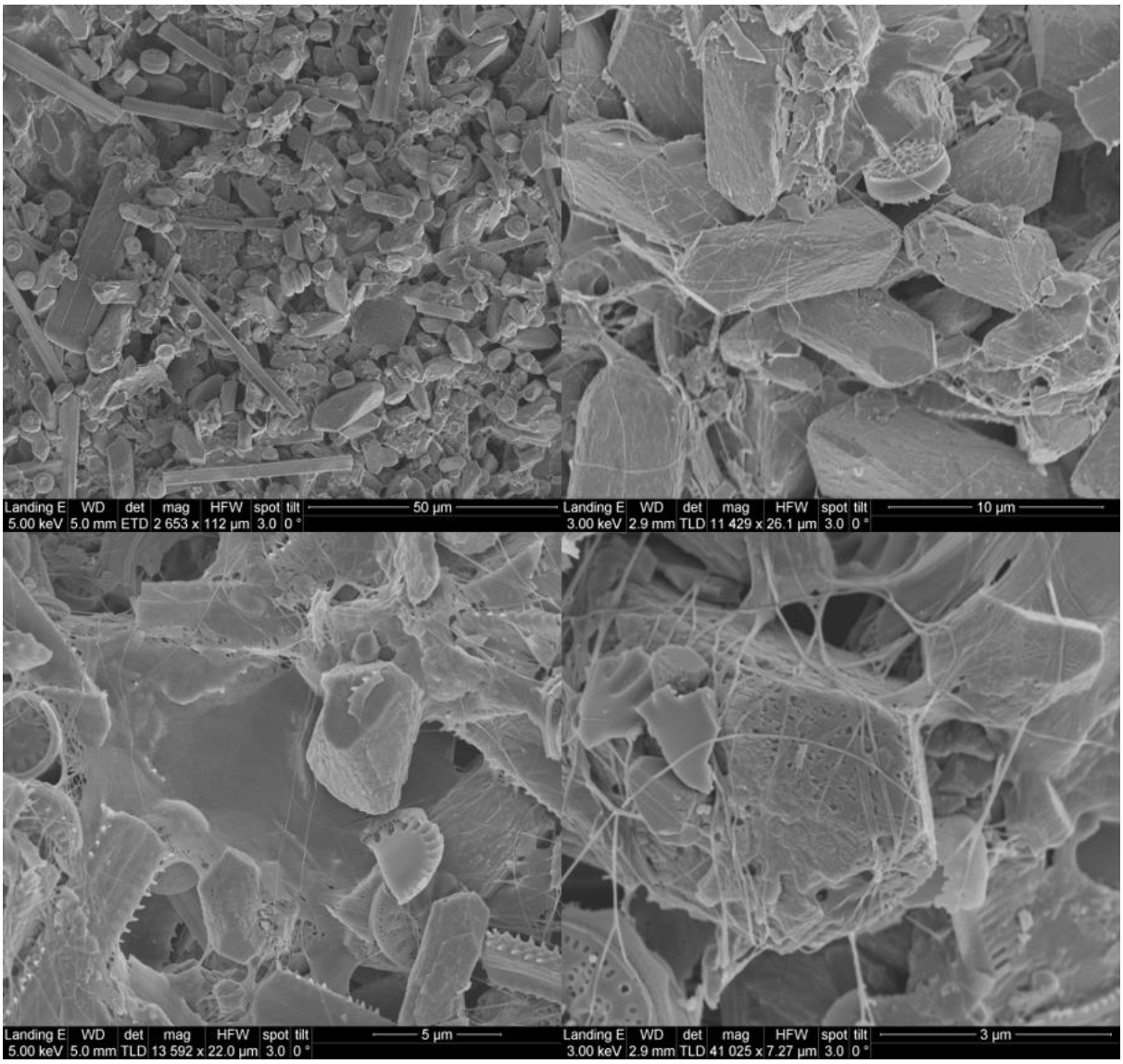

807

808 **Figure S2.** SEM images of FGL whiting particles collected in a sediment trap (July 2017, 13.5 m

809 depth).

810

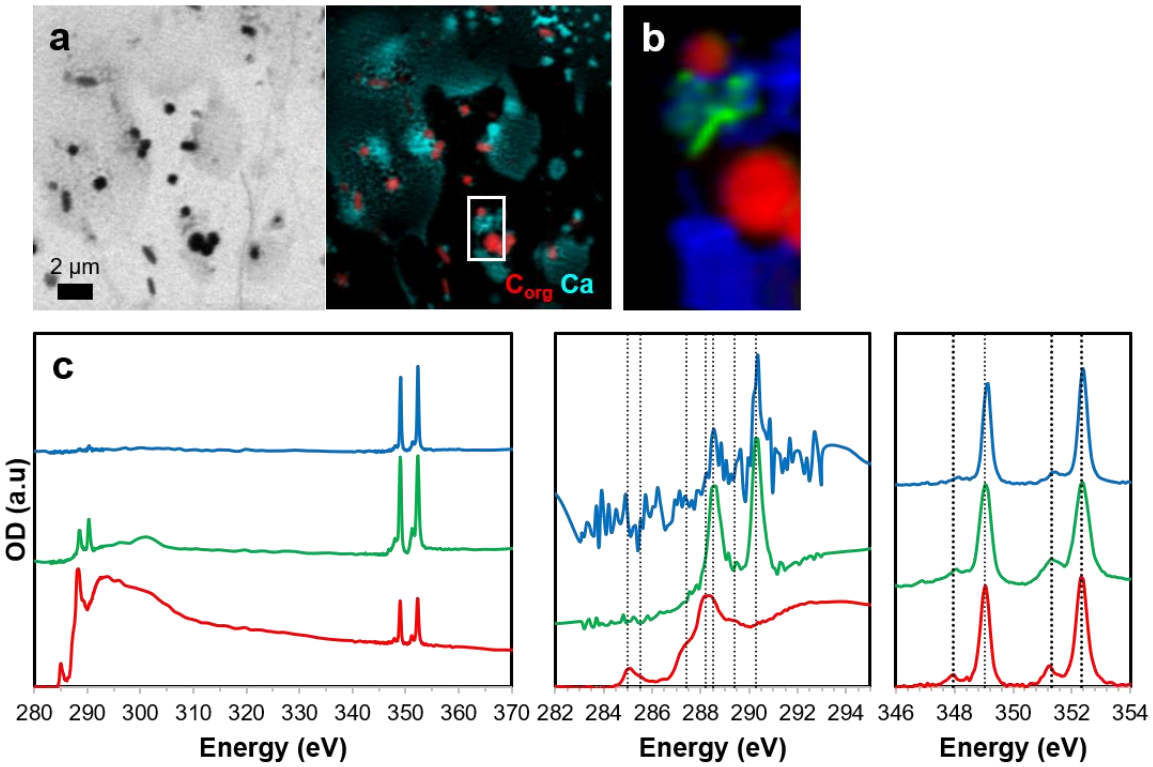

811

812 **Figure S3.** STXM analyses of pre-whiting particulate material from the FGL water column (April,
813 8 m depth). (a) Image obtained at 288.2 eV and corresponding map showing the distribution of
814 organic carbon (red) and calcium (cyan). (b) Map obtained on the area depicted by a rectangle in
815 (a), showing a *Synnechococcus* cell in red, EPS in blue, and ACC particles (green). (c) XANES
816 spectra representative of the *Synnechococcus* cell (in red), EPS (in blue) and ACC particles (in
817 green). C K-edge spectra (middle panel): vertical lines correspond to the absorption energies of
818 different organic functional groups (see main text) and carbonate groups (at 290.3 eV). Ca $L_{2,3}$-
819 edge spectra (right panel): vertical lines correspond to the position of the main peaks in amorphous
820 calcium carbonate. XANES spectra acquired on the EPS (blue spectra) show the presence of
821 adsorbed Ca^{2+} but very weak carbonate signal, while strong carbonate and calcium peaks in the
822 green spectra indicate the presence of calcium carbonate grains, identified as ACC based on
823 splitting ratios (SRL_3 ~ 1.2, SRL_2 ~ 1.4).

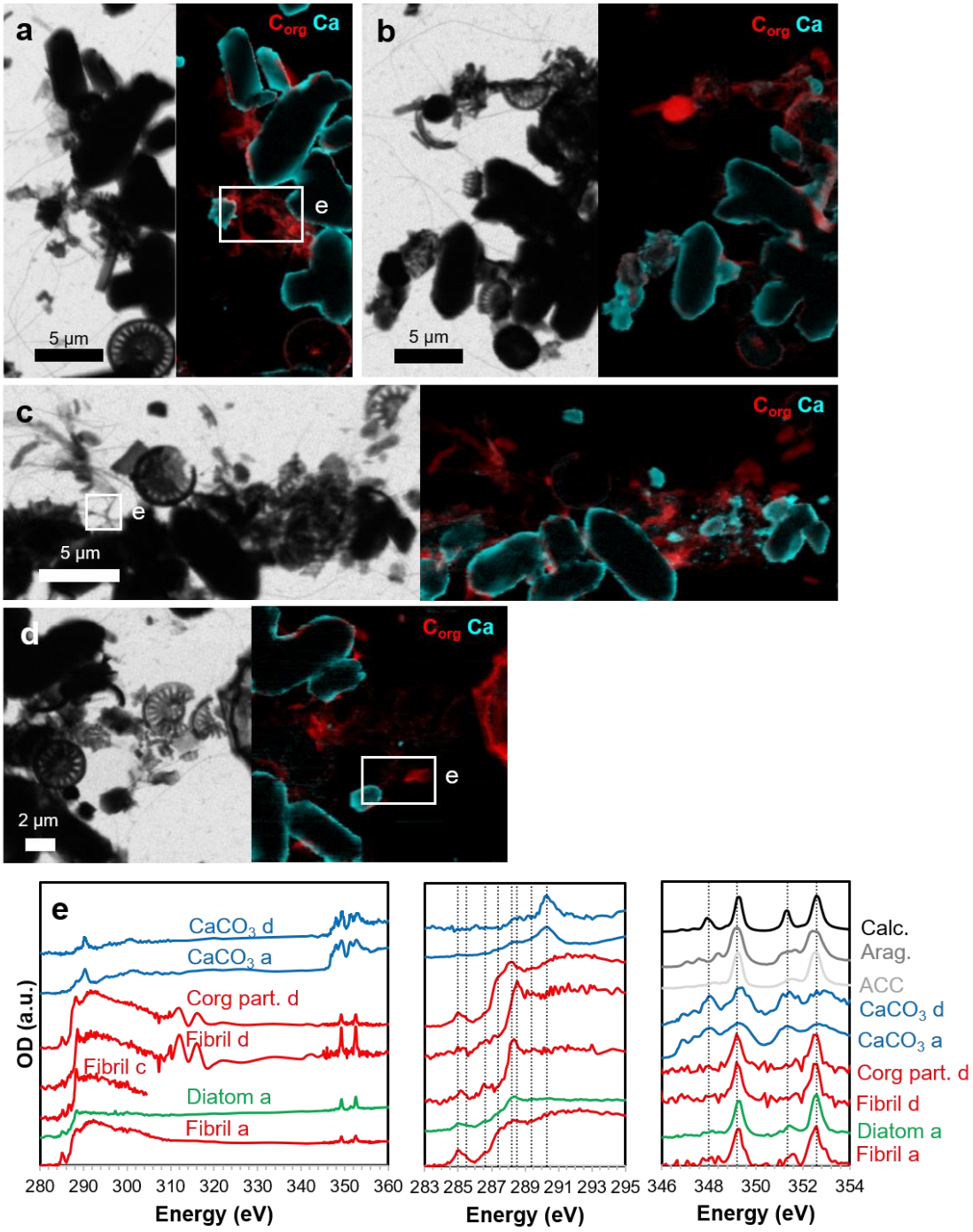

824

825 **Figure S4.** STXM analyses of settling whiting particles collected in a sediment trap

826 (July, 13.5 m depth). (a-d) Images at 288.2 eV (left) and maps of organic carbon (red) and

827 calcium (cyan) (right). The interior of $CaCO_3$ grains sometimes appear black on calcium maps

due the excessive thickness of the grains, causing saturation of the X-ray absorption signal. The white boxes represent the locations of the image stacks from which spectra shown in (e) were extracted. (e) XANES spectra representative of $CaCO_3$ grains in (a) and (d), a dense organic carbon particle in (d), organic fibrils in (a), (c) and (d), and a diatom in (a). Note that for the fibril in (c), the XANES spectrum was only acquired at the C K-edge. C K-edge spectra (middle panel): vertical lines correspond to the absorption energies of different functional groups (see main text). Ca $L_{2,3}$-edge spectra (right panel): vertical lines correspond to the position of the main peaks in the reference calcite (Calc.) spectrum (black). Reference Ca $L_{2,3}$-edge XANES spectra for aragonite (Arag.) and amorphous calcium carbonate (ACC) are also shown.

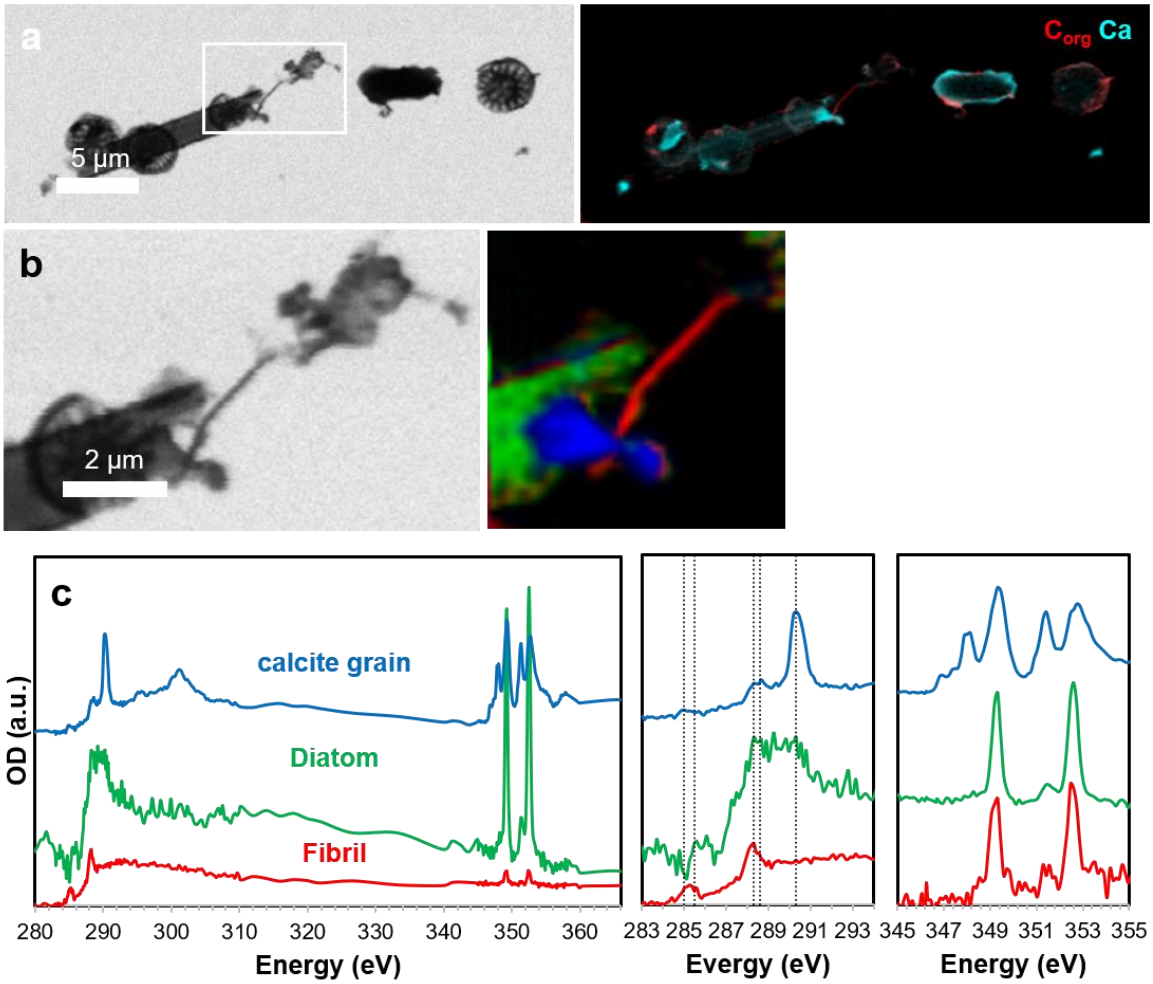

Figure S5. STXM analyses of particles from a FGL sediment core (0-2 inches). (a) Image at 288.2 eV (left) and maps of organic carbon (red) and calcium (cyan) (right). (b) Close-up on the area depicted by a white box in (a). Left: image at 288.2 eV. Right: map showing the distribution of different components extracted from an image stack: a calcite grain (blue), a pennate diatom (green), and an organic filament (red). (c) Corresponding XANES spectra. The vertical lines in the C K-edge spectrum (middle panel) correspond to energy positions of the main absorption features of different function groups (see main text).

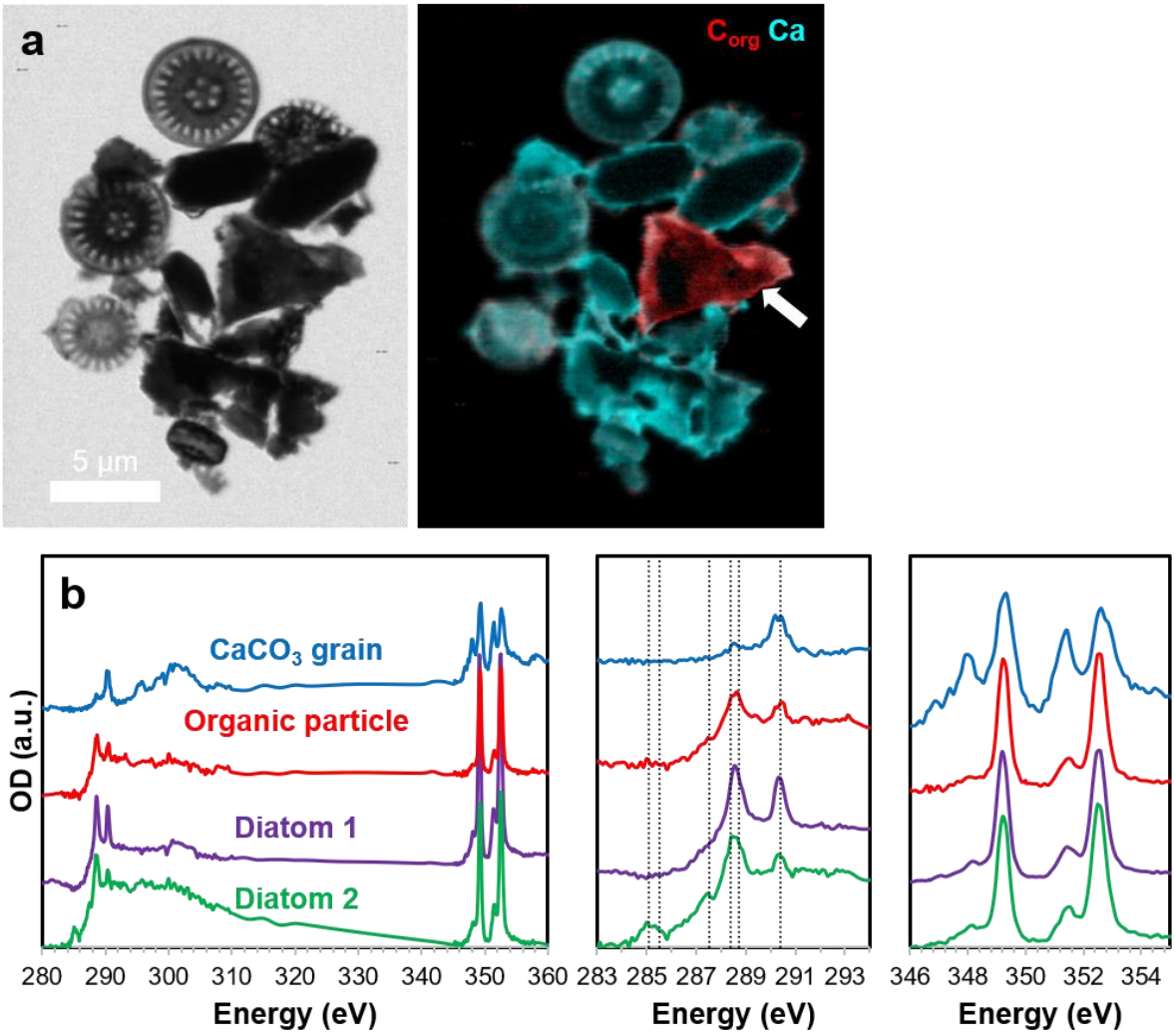

Figure S6. STXM analyses of particles from a FGL sediment core (2-4 inches). (a) Image at 288.2 eV (left) and maps of organic carbon (red) and calcium (cyan) (right). The white arrow points to a dense organic-rich particle. (b) XANES spectra representative of different types of objects in (a): a calcite grain, an organic particle, and two different diatoms. The vertical lines in the C K-edge spectrum (middle panel) correspond to energy positions of the main absorption features of different function groups (see main text).